Available online at www.sciencedirect.com
ScienceDirect
Neuroscience Research 61 (2008) 172–181
Neuroscience Research
www.elsevier.com/locate/neures

# Significance of the deep layers of entorhinal cortex for transfer of both perirhinal and amygdala inputs to the hippocampus

Noriko Koganezawa [a], Ayaka Taguchi [a], Takashi Tominaga [b], Shinya Ohara [a], Ken-Ichiro Tsutsui [a], Menno P. Witter [c,d], Toshio Iijima [a,*]

[a] *Division of Systems Neuroscience, Tohoku University Graduate School of Life Sciences, 2-1-1 Katahira, Aoba-ku, Sendai, Miyagi 980-8577, Japan*
[b] *Department of Neurophysiology, Faculty of Pharmaceutical Sciences at Kagawa, Tokushima Bunri University, 1314-1 Shido, Sanuki, Kagawa 769-2193, Japan*
[c] *Kavli Institute for Systems Neuroscience and Centre for the Biology of Memory, Norwegian University of Science and Technology (NTNU), N-7489 Trondheim, Norway*
[d] *Department of Anatomy & Neurosciences, Institute for Clinical and Experimental Neurosciences, VU University Medical Center, Graduate School of Neurosciences, Amsterdam, 1007 MB, Amsterdam, The Netherlands*

Received 15 February 2008; accepted 21 February 2008
Available online 6 March 2008

**Abstract**

In the rat, a number of sensory modalities converge in the perirhinal cortex (PC). The neural pathway from the perirhinal cortex to the entorhinal cortex (EC) is considered one of the main routes into the entorhinal–hippocampal network. Evidence accumulated recently suggests that EC and PC, far from being passive relay stations, actively gate impulse traffic between neocortex and hippocampus. Using slice preparation maintaining the neurocircuit connecting PC, EC, hippocampal formation and amygdala, we investigated the associative function of PC and EC with respect to sensory and motivational stimuli and the influence of the association on the neurocircuit. In horizontal slices located ventrally to the rhinal sulcus, where we stimulated area 35 and the lateral amygdala, both inputs can be independently conveyed to the dentate gyrus. In slightly more dorsal slices where we stimulated area 36 and the lateral amygdala, the coincidence of the two inputs was needed to activate the hippocampus. This need for association of the two inputs was apparently mediated by the deep layer of EC. In all instances activation of the deep layers of EC was sufficient to activate the dentate gyrus, suggesting the relevance of the deep layers in cortico–hippocampal interactions.


*Keywords:* Entorhinal cortex; Perirhinal cortex; Amygdala; Hippocampus; Signal gating; Optical imaging

## 1. Introduction

The pathway from the perirhinal cortex (PC) to the entorhinal cortex (EC) is one of the two main entry routes for sensory information into the entorhinal–hippocampal network (Burwell and Amaral, 1998; Burwell, 2000; Burwell and Witter, 2002; Witter and Amaral, 2004). Based on our current knowledge of the network it is quite likely that various sensory modalities converge in the rat perirhinal cortex. The perirhinal cortex also interconnects with the amygdala, which plays an important role in various motivational and emotional behaviors (Ono et al., 1995; Nishijo et al., 1998). For its presumed role in declarative memory, the entorhinal–hippocampal system strongly depends on this input from the perirhinal cortex (Eichenbaum et al., 2007). Surprisingly, the projection from PC to EC features a rather unusual high level of inhibition, indicating that transfer of information only occurs when particular requirements are met by the network (de Curtis and Paré, 2004). In view of evidence that memory processing is facilitated by the emotional connotation of the information to be remembered (Cahill et al., 1995, 1996; Hamann et al., 1999; Richardson et al., 2004; Paz et al., 2006), we have previously investigated whether interactions between PC and amygdala may alter the normally inhibited transfer of information into EC. In horizontal slices of the rat obtained near the rhinal sulcus, the neural circuit connecting PC, EC, hippocampal formation, and the lateral nucleus of the amygdala (LA) is largely maintained (Iijima et al., 1994, 1996; Kajiwara et al.,

* Corresponding author. Tel.: +81 22 217 5046; fax: +81 22 217 5048.
*E-mail address:* t-iijima@mail.tains.tohoku.ac.jp (T. Iijima).

0168-0102/$ – see front matter © 2008 Elsevier Ireland Ltd and the Japan Neuroscience Society. All rights reserved.
doi:10.1016/j.neures.2008.02.007

2003). Using such preparations, and optical imaging with a voltage-sensitive dye, we showed that following stimulation in the superficial layers of PC, electrical activity only propagated into EC when sufficient activation occurred in the deep layers of perirhinal area 35. We observed that single stimulation of either PC or LA did not result in sufficient neural activation of the deep layers of areas 35 to provoke activity propagation into EC. However, the deep layers of area 35 were depolarized much more strongly when the two stimuli were applied simultaneously, resulting in spreading activation in EC. Our observations suggested that a functional neural basis for the association of higher-order sensory inputs and emotion-related inputs exists in PC and that transfer of sensory information to the entorhinal–hippocampal circuitry might be affected by the association of that information with incoming information from the amygdala (Kajiwara et al., 2003; Pelletier et al., 2005).

In our previous study, focus was on slices obtained dorsal to or at the rhinal sulcus, to ascertain that both areas 36 and 35 were present in the slice. Our previous findings that perirhinal area 35 was critically involved in the transfer of activity into EC are in line with anatomical data (Burwell and Amaral, 1998). Therefore, in this study, we conducted experiments in horizontal slices obtained at levels through and ventral to the rhinal sulcus such that the slices would maintain the connectivity between area 35 and the entorhinal cortex. In these preparations we observed that in some slices the neural activity evoked in the superficial layer of PC or in LA may conduct independently to the hippocampus. In this propagation of neural activity, the deep layers (V/VI) of the rhinal cortices appeared to play an important role. In some other slices, the association of the cortical input and amygdala input was essential to cause the activation of the hippocampus as seen in the previous study. In such slices, the association of these two different inputs most probably occurred in the deep layer of EC. Therefore, we conducted a whole-cell voltage clamp in the layer V neurons of EC, and found that in the deep layers of EC cells apparently receive both cortical input and amygdala input. Taken together, our findings indicate that the deep layers of EC are part of the network that integrates cortical and amygdala inputs and submits the resulting information to the dentate gyrus.

## 2. Materials and methods

### 2.1. Slice preparation and solutions

Male Wistar rats (100–160 g) were deeply anesthetized by ether and decapitated. Slices (400 μm thickness) were prepared using a vibratome (DTK-3000W, Dosaka, Japan) in ice-cold sucrose artificial cerebrospinal fluid (s-ACSF) (Moyer and Brown, 1998). The s-ACSF was composed of (in mM) 248 sucrose, 5 KCl, 1.25 $NaH_2PO_4$, 2 $MgSO_4$, 1 $CaCl_2$, 1 $MgCl_2$, 22 $NaHCO_3$, and 10 D-glucose, and oxygenated with a mixture of 95% $O_2$–5% $CO_2$, pH 7.4, chilled to 4 °C. The slices including the PC, EC, hippocampal formation and amygdala were cut at an angle indicated by line *h* shown in Fig. 1A. For this, the hemispheres were separated and their dorsal part removed by razor cuts parallel to line *h*, and each hemisphere was glued with its dorsal cut surface to a vibratome stage. Fig. 1B shows an example of a Nissl-stained slice cut at the level of line *h*. With the use of such slices, we investigated

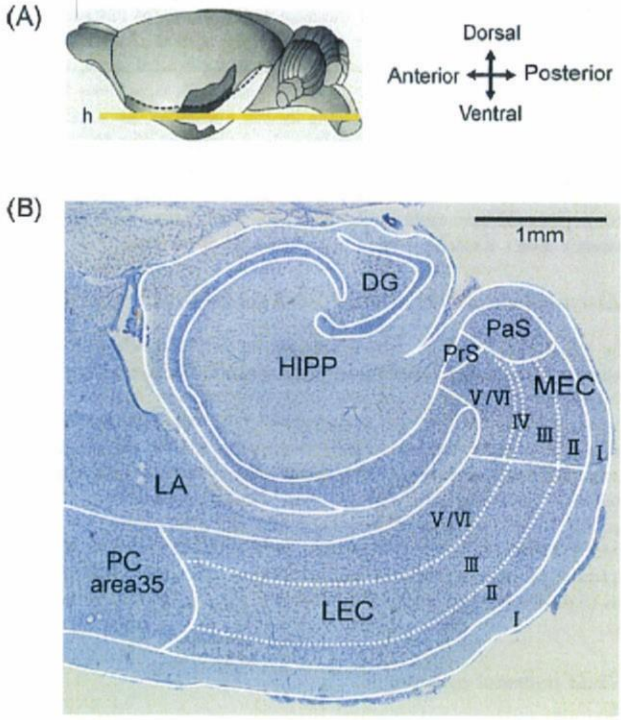


Fig. 1. Preparation of the rat brain slice. (A) Lateral view of the rat brain. Approximate orientation of the brain slice is illustrated by line *h*. (B) Nissl-stained slice. The slice includes the hippocampus (HIPP), medial and lateral entorhinal cortex (MEC, LEC), perirhinal cortex (PC), and lateral amygdaloid nucleus (LA).

propagation of neural activity following stimulation of perirhinal layers II/III and of the amygdala.

Before the start of recording, slices were submerged in the incubation chamber with standard ACSF for more than 1 h. The standard ACSF used for incubation and recording consists of (in mM) 124 NaCl, 5 KCl, 1.25 $NaH_2PO_4$, 2 $MgSO_4$, 2 $CaCl_2$, 22 $NaHCO_3$, and 10 D-glucose, oxygenated with a mixture of 95% $O_2$–5% $CO_2$, pH 7.4. The ACSF was maintained at room temperature (26–28 °C).

### 2.2. VSD (voltage-sensitive dye) imaging

The optical recording methods were similar to those reported elsewhere (Barish et al., 1996; Iijima et al., 1996; Kajiwara et al., 2003). For recording, a slice was submerged in a recording chamber mounted on a fluorescence macro zoom microscope (MVX-10, Olympus, Japan). The slice was stained in the recording chamber for 3 min with the voltage-sensitive dye RH-795 (0.5 mg/ml ACSF). The voltage-sensitive dye has excitation and emission maxima at 530 and 712 nm, respectively. Emission decreases proportionally to the changes of membrane depolarization (Grinvald et al., 1994). After the staining, extra dye was washed out with oxygenated superfusion solution and the preparation was incubated in the recording chamber for another 10–15 min before the optical measurements were performed. The magnification of the microscope was adjusted to 2.8×–3.3×, depending on the size of the objective field on the slice preparation. Illumination from a tungsten–halogen lamp (150 W) was passed through a heat filter (<10% transmittance for 700–1600 nm light). The excitation light filtered at 535 nm (±20 nm band-pass) was reflected down onto the preparations by a dichroic mirror (halfreflectance wave length of 580 nm). Epifluorescence through a long-wavelength pass filter (50% transmittance at 600 nm) was detected with a complementary metal oxide semiconductor sensor array detector (MiCAM Ultima L-camera, BrainVision, Japan; 100 μm × 100 μm pixel size, 100 × 100 pixel array). By using this optical imaging system, we acquired 512 frames at a rate of 0.5 or 1.0 ms/frame. To represent the spread of neural activity, we superimposed color-coded optical

signals on the bright-field image of the slice or the image of Nissl-stained preparation made from the brain slice subjected to the optical imaging. In this procedure, we applied a color code to the fraction of the optical signal, which exceeded the baseline noise. That is, optical signals with sizes close to the baseline noise were ignored. For reducing the baseline noise, we sometimes averaged eight identical recordings acquired with a 3 s interval. The data set was averaged in the frame memory directly. The optical signal was analyzed off-line using custom-made software or BrainVision analyzer software. Changes in membrane potential were evaluated as DF/F (F − Fo/F, where Fo is the base fluorescence level). Recordings were made in a total of 29 slices.

### 2.3. Electrical stimulation to the PC and the amygdala

The stimulating electrode was a tungsten bipolar electrode with a tip separation of 150 μm. Since anatomical studies indicate that layers II/III of the PC receive projections from sensory areas (Burwell and Amaral, 1998; Faulkner and Brown, 1999), we placed the stimulus electrode for the PC on layers II/III to mimic input from the sensory cortices to the PC. We placed another stimulating electrode in the lateral amygdaloid nucleus (LA) to mimic an emotional input. Initially, a single-pulse electrical stimulation of 80–100 μA for 300 μs was used. If the single stimulation was found not to be sufficient to cause measurable activation in the PC or EC in the VSD imaging, we replaced the single stimulation with a repetitive stimulation at 40 Hz for 100 ms (5 pulses at 25 ms interval), each current pulse being 80–100 μA for 300 μs.

### 2.4. Field potential recording

A glass recording electrode filled with normal medium (5–10 MΩ) was used. The field potential was filtered at 1 kHz low-pass filter, amplified (MEZ-8300, Nihonkoden, Japan), and digitized with the use of the optical imaging system through its external input terminal. The field potential was continuously monitored throughout the experiment, and no photodynamic effect on its amplitude was observed by the optical recording.

### 2.5. Slice-patch recording

Synaptic responses were recorded in the layer V neurons of LEC with a whole-cell voltage clamp *in vitro* when either PC or LA, or both PC and LA were stimulated. We made patch clamp recordings on pyramidal-like neurons, although we did not identify the species of neurons precisely in this study. For slice patch recordings each slice was transferred onto a fine-mesh membrane filter (Omni Pore membrane filter, JHWP01300, Millipore, USA) held in place by a thin plexiglas ring (inner diameter, 11 mm; outer diameter, 15 mm; thickness 1–2 mm; Tominaga et al., 2000). Slices placed in the plexiglas ring were transferred to a moist holding chamber continuously supplied with a moistened mixture of the 95% $O_2$, 5% $CO_2$ gas mixture. After 1 h of incubation in this chamber, a slice on the holding ring was transferred onto an experimental chamber placed on a fixed stage and subjected to the experiments. Patch-clamp recordings in the whole-cell mode were made using a patch-clamp amplifier with a capacitive headstage (Axoclamp 200B, Axon Instruments, USA) using pipettes (3–5 MΩ) of borosilicate glass (Sutter Instruments, USA) pulled using a P-97 Flaming–Brown pipette puller (Sutter Instruments, USA). Whole-cell recordings were low-pass-filtered at 3 kHz and digitized at 10 kHz. Data were digitized with a digitizer (Digidata 1342, Axon Instruments, USA) and fed into a computer for off-line analysis (Next Computer) using software AxoClamp 9.0 (Axon Instruments, USA). Electrical stimulations were applied by constant current pulses (SS-202J with SEN-7203, Nihonkoden, Japan) through a bipolar tungsten electrode placed in layer II/III of PC and LA. Stimulation was given for 300 μs and the intensity was varied in the range of 80–100 μA to obtain EPSCs. Neurons were visualized by oblique illumination with the aid of the contrast enhancement of a CCD-camera (C2741, Hamamatsu photonics, Japan) mounted on an upright microscope (Axioskop 2FS, Ziess, Oberkochen, Germany). In voltage-clamp mode, a test membrane potential step (−10 mV) was always applied prior to electrical stimulation, and traces with series resistance lower than 20 MΩ were accepted. The pipette solution consisted of, in mM: 130 Cs-$MeSO_3$, 10 Hepes, 4 $MgCl_2$, 4 NaATP, 0.4 NaGTP, 10 Na-Phosphocreatine, 10 EGTA; pH was adjusted to 7.2.

### 2.6. Drugs

The entorhinal cortex has been reported to harbor many more cells containing the calcium-binding protein parvalbumin than is the case for the PC. Since it has been well established in these areas that parvalbumine colocalize for 100% with GABA, it is likely that, in the EC, more GABA-containing cells will be present compared with the PC (Burwell et al., 1995; Miettinen et al., 1996; Wouterlood et al., 2004). To investigate the spatiotemporal distribution of excitatory activities between the PC and the entorhinal–hippocampal circuit, synaptic inhibition was partly suppressed by applying a low concentration of the GABAA antagonist bicuculline (1–2 μM) ((−)-bicuculline methiodide, Sigma–Aldrich Co., USA) in the recording solution as reported previously (Kajiwara et al., 2003). Under such conditions, the optical imaging with voltage-sensitive dye has already measured spread of neural activity in the entorhinal–hippocampal network elicited by electrical stimulation to LEC in rat brain slices without inducing spontaneous paroxysmal activities (Iijima et al., 1994, 1996).

### 2.7. Histology

The brain slices of 400 μm thickness were fixed with 4% paraformaldehyde for more than 1 week. Subsequently, the slices were stored in PBS with 30% sucrose for more than 10 h and cut at 50 μm thickness with the use of a freezing microtome (SM-2000R, Leica Microsystems, Germany). Sections were Nissl-stained in 0.25% thionin solution. Fig. 1B shows the histological result. The areas of the perirhinal and entorhinal cortices were delineated on the bases of cytoarchitectural criteria (Burwell et al., 1995; Insausti et al., 1997). In the perirhinal cortex, we differentiated between areas 35 and 36 and for the entorhinal cortex a division into lateral entorhinal cortex (LEC) and medial entorhinal cortex (MEC) was used. By comparing these histological data with the optical imaging data, we could identify the region in which neural propagation occurred. In some analyses we superimposed the spatio-temporal activation pattern detected with VSD imaging onto the Nissl-stained preparation obtained from that same slice as shown in Fig. 2.

## 3. Results

### 3.1. Propagation of neural activity evoked in the superficial layer of the PC or in the amygdala

In this study horizontal slices were obtained through the ventral part of the rat brain, below and apart from the rhinal sulcus for at least 300 μm (Fig. 1A). Fig. 1B shows a Nissl-stained example of the slices used in this study. The slice preparations contained the PC, EC, hippocampal formation, and amygdala. In all our slices we noticed that both LEC and MEC were present, and could be easily distinguished. Since we aimed for slices directly ventral to or including the ventral bank of the rhinal sulcus, area 36 was expected not to be present. In some of our slices, however, area 36 was still present, most likely due to a slightly different cutting angle, and in those instances our stimulation site quite generally was in area 36. Note that during the course of the imaging experiments, it was hard to confirm the structure of the perirhinal cortex. So, we examined the site of stimulation afterwards, based on the cytoarchitecture as revealed by the Nissl-stained preparation of the slice subjected to the VSD imaging.

First we investigated propagation of neural activity following stimulation of layers II/III of PC (hereafter a PC stimulation) which mimics a sensory input, and stimulation of the lateral amygdala which mimics an emotional input (hereafter an LA stimulation). In Fig. 2A and D, the spatio-temporal propagation pattern of neural activity evoked by the PC stimulation (Fig. 2A)

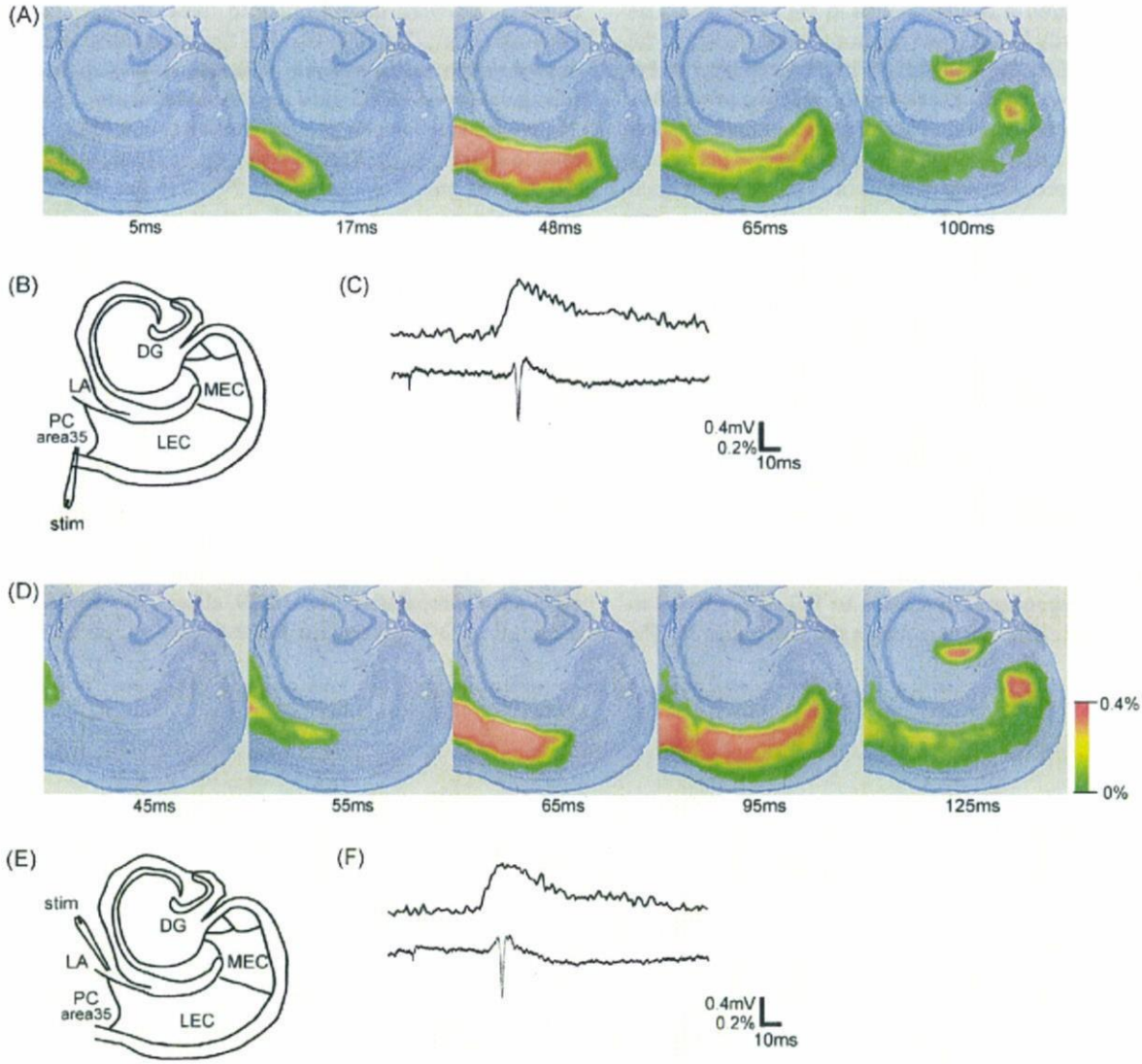


Fig. 2. (A, D) Propagation of the evoked activity in the superficial layer of PC (A) and in LA (D). To represent the spread of neural activity, the color-coded optical signal was superimposed on the image of Nissl-stained preparation made from the brain slice subjected to the optical imaging. (B, E) Arrangement of the stimulating electrode. (C, F) Simultaneous recordings of an optical signal (upper trace) and a field potential (lower trace) in the dentate gyrus.

or by the LA stimulation (Fig. 2D) is shown respectively. A single pulse stimulation (Section 2) was used in each recording. In these figures we superimposed the propagation pattern of neural activity obtained with VSD imaging on the image of Nissl-stained section obtained from the brain slice which was subjected to the VSD imaging experiment. The simultaneous recordings of the optical signal change and the field potential change in the dentate gyrus of the hippocampal formation (DG in Fig. 2B and E) associated with the PC stimulation or LA stimulation are shown in Fig. 2C and F, respectively.

When a single stimulation was applied to the superficial layer of the PC at 0 ms in Fig. 2A, evoked activity spread at 17 ms to the superficial layer of EC beyond the PC/EC border, which seems to be consistent with the anatomical observation that the perirhinal projection to the entorhinal cortex terminates mainly in layers II and III (Burwell and Amaral, 1998). In all slices subjected to the VSD imaging (29/29), we did not observe any amygdala activation following stimulation of superficial layer of entorhinal cortex. After 17 ms, the domain of the activity appeared to move to the deep layer of the EC (48 ms). The activity subsequently spread medially in the deep layers of EC (65 ms). It is reported that inhibition, mediated by GABA, is more pronounced in layer II than in layer V (Berretta and Jones, 1996; Wood and Jones, 1998; Woodhall et al., 2005). The fundamental differences of the inhibitory systems in deep and superficial layers of the EC may thus cause the spread of neural activity to occur mainly in the deep layers of the EC. The neural activity evoked in the superficial layer of the PC was finally propagated the DG (Fig. 2A, 100 ms). The activation of a part of the deep layers of the EC, near the border of LEC and MEC as shown in the pattern of 100 ms, always preceded the activation of the DG. The field potential recording in Fig. 2B clearly shows that not only population EPSPs but also population spikes were generated in the DG.

The LA stimulation was also applied in the same slice. The evoked neural activity in LA came out from the amygdala to the deep layer of PC, then spread medially in the deep layer of PC and EC (Fig. 2D, 45, 55 ms), and finally reached to the DG. Simultaneous recording in Fig. 2F also shows that the excitation caused in DG was strong enough to generate action potentials. If we compare the propagation patterns in Fig. 2A and D, each propagation pattern appeared to be quite similar. Twenty nine horizontal slices, taken at the ventral level as specified, were subjected to the VSD imaging study for analyzing the propagation of neural activity. The propagation patterns as shown in Fig. 2 were observed in 12/29 slices. In all 12 slices, histological assessment of the slice afterwards revealed that the site of stimulation was in area 35.

### 3.2. *Associative stimuli to the PC and the amygdala*

In some other slices used in this experiments (7/29), only co-activation of PC and LA, with individual stimuli being applied within a certain critical interval, resulted in the activation of DG (Fig. 3C), and independent stimulation to PC or LA failed to activate DG. In all 7 cases, the stimulation site was in area 36. The observations were quite similar to those reported previously (Kajiwara et al., 2003). In Fig. 3, a typical example is shown. In this particular slice, a single stimulation was applied to the superficial layers of PC and a repetitive stimulation (5 stimuli at 25 ms interval: Section 2) was applied to LA (Fig. 3D). The evoked activity in the superficial layers of PC expanded beyond the area of initial excitation in PC, and the excitation was propagated to almost the whole extent of LEC at 80 ms after stimulation (Fig. 3A). However no activation was observed in MEC and in the hippocampal formation in the recordings after this period. Similarly, the activation of LA, which was followed by the activation of PC and successive activation of LEC, also failed to spread beyond the border of LEC and MEC (Fig. 3B). However, when a single stimulation was applied to the superficial layer of PC 60 ms after the start of the application of a repetitive stimulation to LA, the excitation spread beyond the border of LEC and MEC and finally DG was activated (Fig. 3C).

The critical interval of the delivery of two stimuli had a variation in each experiment, although the optimal interval which resulted in the maximum response in DG was constant in each slice preparation. In 10/29 slices, no activation was observed in DG, even when PC and LA were co-activated.

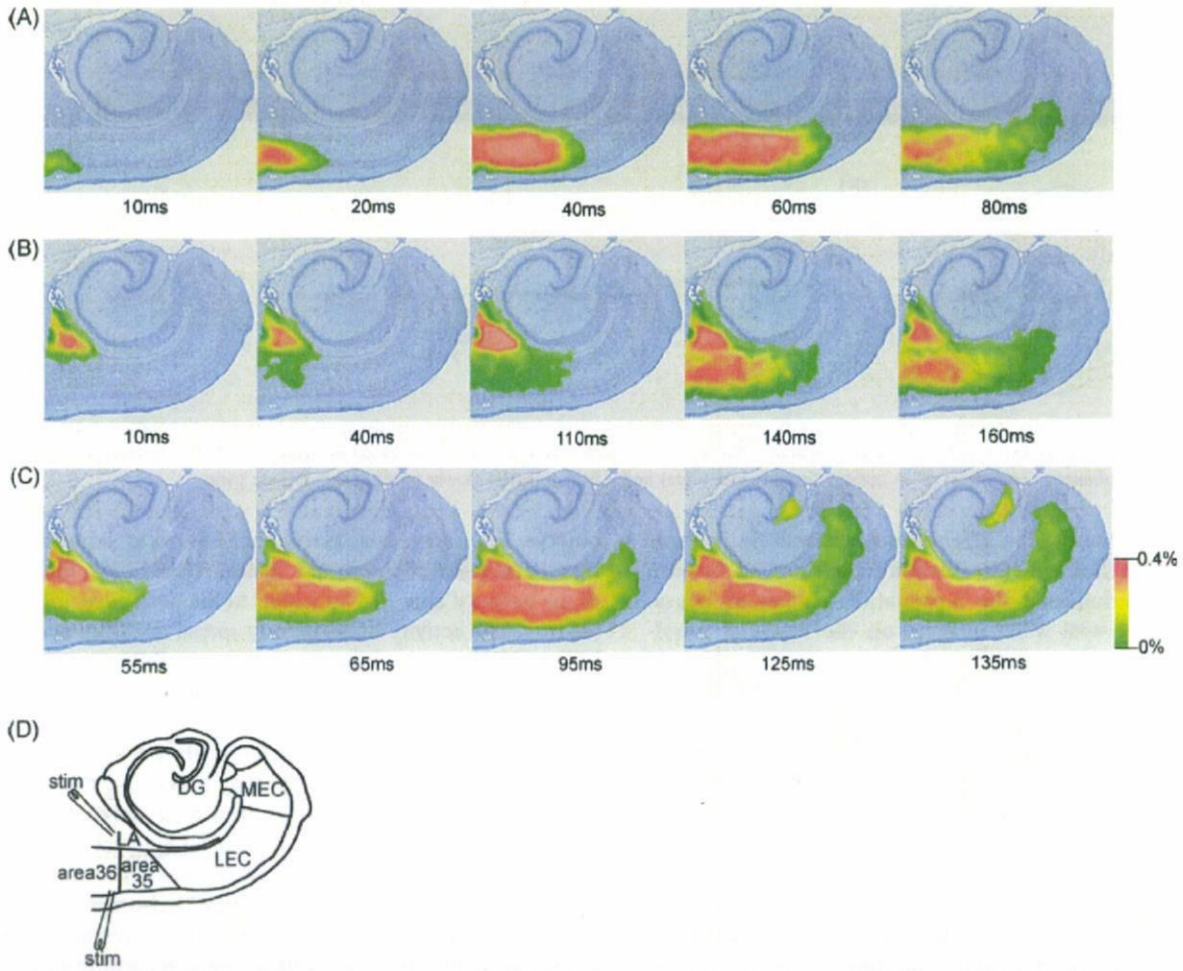


Fig. 3. Propagation of neural activity in the slice preparation. The neural activity was evoked by the stimulation of the superficial layer of PC (A) or of LA (B), or co-stimulation of LA and PC (C). (D) Arrangement of the stimulating electrodes.

### 3.3. Interaction of the cortical pathway and amygdala pathway

These results thus indicate that the transfer of information from amygdala and perirhinal cortex may occur in an independent as well as dependent manner and that the outcome most likely depends on the dorsal to ventral level of the slice, implying a different efficacy for perirhinal areas 35 and 36, as well as for more dorsal and ventral domains of the lateral nucleus of the amygdala. This does not exclude the possibility that even in the situation that the two inputs do result in dentate activation independently, they do interact when applied simultaneously. That such interaction may take place is quite likely in view of the consistent observation that activation in the dentate gyrus, when taking place, was always preceded by activity increases in the deep layers of the entorhinal cortex, irrespective of the stimulation protocol that was used. This thus suggests that the deep layers of the entorhinal cortex may hold a relevant portion of the neural circuitry for both inputs to reach the dentate gyrus. The potential role of the deep layers was therefore further studied.

If the two neuronal pathways are absolutely independent, individual neural activations caused in the rhinal cortices by PC stimulation or by LA stimulation are expected to be independent as well and the changes in signal should reflect that. In VSD imaging, each pixel of an image sensor records the sum of the membrane potential changes of every membranous structure projected onto the pixel. Thus, fluctuations of the optical signal from baseline represent the sum of membrane potential changes (Grinvald et al., 1982). Then we can compare the size of the evoked neural events, or more correctly the size of total membrane potential changes associated with neural activity in the different stimulation protocols, assuming that in all instances the contribution of glial cells to the signal will be constant (Otsu et al., 2000). To test whether the signal changes evoked by stimulations of the two pathways are independent or not, we measured the size of neural events in the deep layer of the rhinal cortices when the activities are evoked by only PC stimulation, by LA stimulation only, and by the co-stimulation of PC and LA (Fig. 4A and B). Then we compared the mathematical sum of the measured responses to the responses associated with the co-stimulation of PC and LA (Fig. 4C). We hypothesized that if the cortical and amygdala pathways are absolutely independent, the mathematical sum of the size of neural event associated with only PC stimulation and that associated with only LA stimulation would be almost equal to the size of neural event associated with the co-stimulation of PC and LA. As shown in columns 1–12 of Fig. 4C (corresponds to number of sample points 1–12 as seen in Fig. 4A), this is not the case. That is, a non-linearity is seen over all of the columns. In columns 1–6, the sum of the responses associated with the two single stimulations exceeds that associated with the co-stimulation of PC and LA. In contrast, in columns 7–10, the situation is totally reversed. Here, the magnitude of the measured signal changes associated with co-stimulation of PC and LA exceeds the sum of the individually evoked responses. This means that the simultaneous stimulation of the two inputs strengthened the overall neural excitation in these regions. This effect may further cause the additional excitations in the regions of 11 and 12, although no excitability was measured in these areas following independent stimulations of PC or of LA (Fig. 4B, traces in 11 and 12). The associative effect was most prominent in the deep layers, compared to the effect observed in the superficial layers using the same procedure (data not shown). We have performed the same analysis as shown in Fig. 4 on seven slices, and obtained similar result in each slice.

### 3.4. Integration of cortical and amygdala inputs

The results shown in Fig. 4 strongly suggest that the cortical and amygdala pathways into the entorhinal–hippocampal system share at least parts of their neurocircuits, mediating integration of the two inputs. Such integration appears to strengthen the overall neural response, resulting eventually in the transfer of neural activity to the dentate gyrus. The sampling points of the data represented in columns 7–10 (Fig. 4) are in the deep layers of the medial part of LEC and the adjacent part of MEC. It has been reported that neurons of LA project, among others, to layer V neurons in LEC (Krettek and Price, 1977; Pikkarainen et al., 1999; Rosenkranz and Johnston, 2007). When combining all these data, it is most likely that the integration of the two inputs takes place in the deep layers of LEC, although it cannot be excluded that the perirhinal areas 35 and 36 may mediate integration as well.

To examine the possibility that the integration is mediated by the neurons in the deep layers of LEC, we performed patch-clamp recordings in visually identified layer V neurons in the medial part of LEC. In individual experiments, we tried to record the synaptic current from the same neuron while either PC or LA, or both were stimulated. We made whole cell recordings in 16 cells and found that all of them respond to each stimulation, indicating that they receive both cortical and amygdala inputs. In Fig. 5, a typical result is shown. In the upper panel, ten consecutive recordings are superimposed. In A and B, only PC or LA was stimulated respectively, while PC and LA were co-stimulated in C. In this particular case, the cell sometimes failed to respond to LA stimulation. In other cells, such failures were also observed following PC stimulations. However, every neuron in the deep layer of the entorhinal cortex which was subjected to the patch-clamp recordings did not fail to respond to the associative stimulation at all. This appears to be the effect of integration of the two inputs which is expected to strengthen the synaptic connectivity. Where the integration does occur remains to be clarified. In the lower panel a typical EPSC was selected from the EPSCs shown in the upper panel. The amplitudes of the averaged as well as of single EPSC for both the single PC and LA stimulation are not significantly different from those seen after co-stimulation of both inputs. The EPSCs obtained from other neurons had a similar nature as those shown in Fig. 5.These findings indicate that single cells are not likely to receive both inputs but the fact that all these cells responded to both inputs is taken to support the concept that the network comprising neurons in layer V of LEC is integrating these two inputs as to provide active transfer to DG.

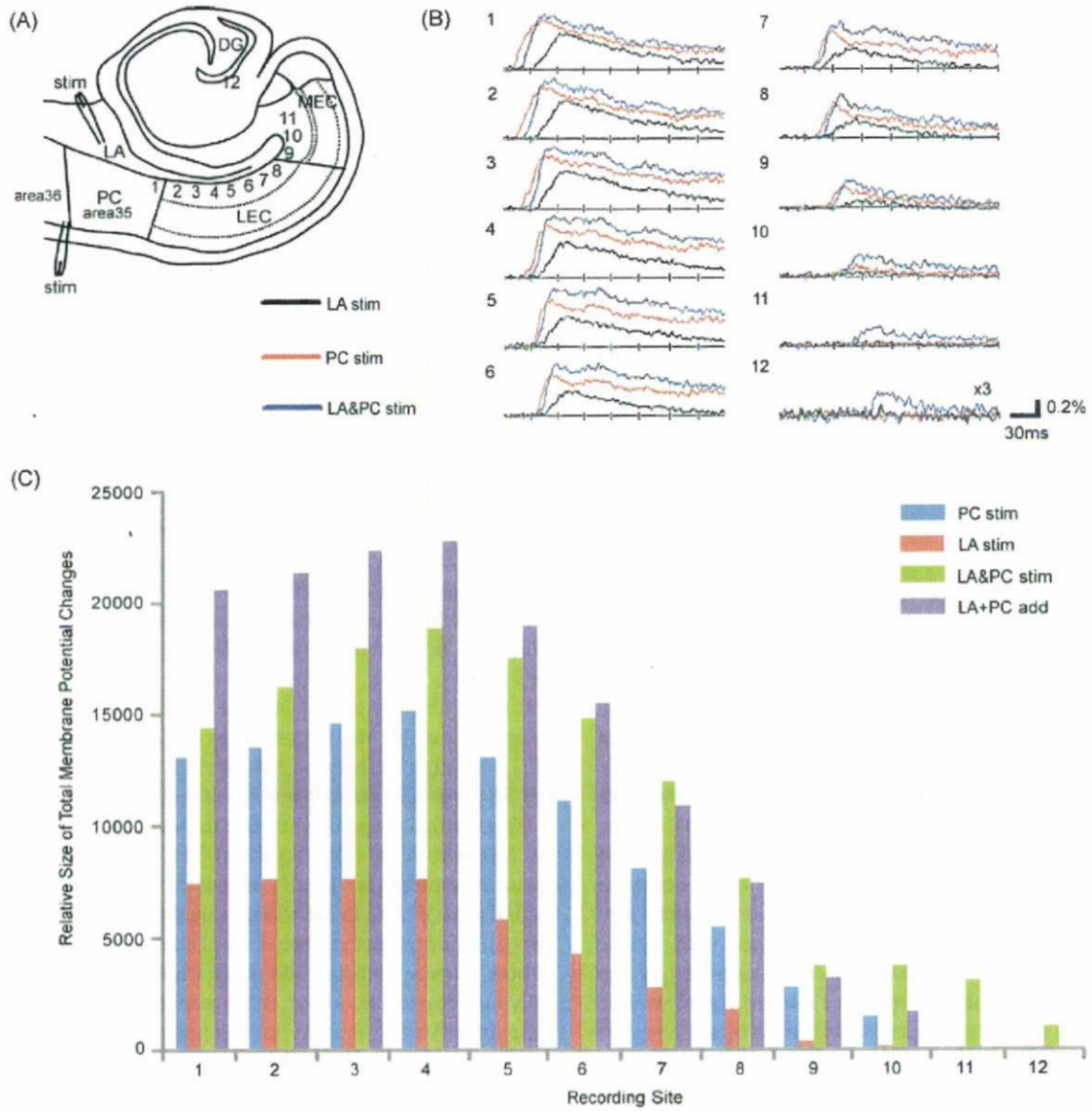


Fig. 4. Comparison of total membrane potential changes in various sites of the deep layer of rhinal cortices and the dentate gyrus caused by PC or LA stimulation, or co-stimulation of LA and PC. (A) Arrangement of stimulating electrodes and the sites (1–12) from which optical signals in (B) were collected. Each optical signal was measured from an area of 300 $\mu m^2$. (B) Optical signal traces obtained from the sites of 1–12 shown in (A). In each group of record (1–12), the optical signal trace of red was obtained by PC stimulation, black by LA stimulation and blue by co-stimulation of LA and PC. In 12, signals were shown by 3-fold magnification. (C) Relative sizes of total membrane potential changes. Number of column (1–12) represents the site of recording in (A). In each column, applied stimulations were represented with different colors. PC stimulation; blue, LA stimulation; red, co-stimulation of LA and PC; green, and the mathematical sum of the size of PC stimulation and LA stimulation; purple.

## 4. Discussion

The parahippocampal cortex, comprised of the perirhinal, postrhinal and entorhinal cortices, is the gateway to the hippocampus. It is critically involved in complex functions, such as memory, object recognition, sensory representation and spatial orientation (Suzuki and Eichenbaum, 2000; Murray and Richmond, 2001; Witter and Wouterlood, 2002). A number of sensory modalities most likely converge in the rat perirhinal cortex. The neural pathway from the perirhinal cortex to the entorhinal cortex is considered one of the main paths into the entorhinal–hippocampal network (Burwell and Amaral, 1998; Burwell, 2000; Burwell and Witter, 2002; Witter and Amaral, 2004). In horizontal slices of the rat brain near the rhinal sulcus, the neural circuit connecting the PC, EC, hippocampal formation and amygdala is preserved (Iijima et al., 1994, 1996; von Bohlen und Halbach and Albrecht, 2002; Kajiwara et al., 2003). Using such preparations, in a previous study we reported on the potential associative function of deep layers of perirhinal area 35 with respect to sensory and motivational stimuli and the influence of this association on the perirhinal–entorhinal–hippocampal neurocircuit (Kajiwara et al., 2003). In the present study, we conducted similar experiments with horizontal slices dissected out just ventral to the rhinal sulcus,

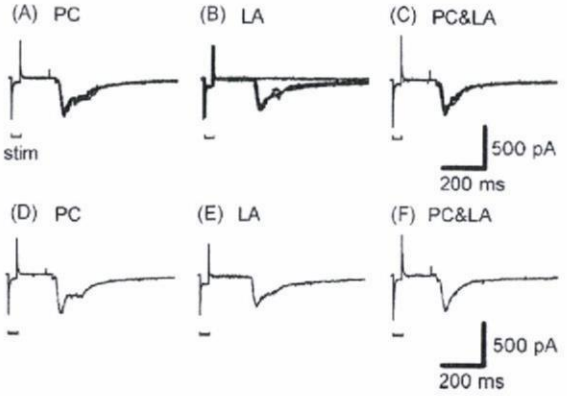


Fig. 5. Recordings of EPSCs from a neuron in layer V of LEC. Upper panel represent the typical EPSCs obtained from the same cell when the stimulation was applied to the superficial layer of PC (A), LA (B), and both LA and PC (C). Ten consecutive recordings are superimposed in (A)–(C), respectively. In the lower panel, a typical EPSC was selected from the EPSCs shown in the upper panel. In every experiment, the superficial layer of area 35 was stimulated.

as to maintain the circuitry between area 35 and the entorhinal cortex. This was achieved in 12/29 (41%) of the slices. In all these slices we found that the neural excitation caused either in the superficial layer of area 35 or in LA was successfully conducted to the dentate gyrus of the hippocampus and generated action potentials. We further observed that the transfer of neural activity from the superficial layers of area 35 or LA to the dentate gyrus, is mediated by the circuits in the deep layers V/VI of the entorhinal cortex.

Increasing attention is being paid to the role of the entorhinal cortex as a dynamic processor of information both entering and leaving the hippocampus. Evidence accumulated recently suggests that the EC and the perirhinal cortex, far from being passive relay stations, actively gate impulse traffic between neocortex and hippocampus, because they are endowed with a powerful intrinsic inhibitory system. It is proposed that the cross-talk between the PC and EC is not organized to unrestrictedly transfer information, but to select relevant inputs (de Curtis and Paré, 2004; Woodhall et al., 2005). The critical question is how the inhibitory control of perirhino–entorhinal communication is regulated, and how it influences the reciprocal information transfer between the neocortex and the hippocampus. The extrinsic excitatory inputs might overcome the local inhibition by causing a sufficient depolarization of projection cells. Another likely possibility is that they activate a subgroup of GABA interneurons that inhibit other GABA cells (Pelletier et al., 2005; Pinto et al., 2006), comparable to what has been demonstrated in the hippocampus, where calretinin-positive hippocampal interneurons only contact other interneurons (Gulyás and Freund, 1996). As a result, excitatory afferents to these local circuit cells would produce a disinhibition of principal projection cells.

In 7 slices out of 29 (24%), single stimulations in either PC or LA did not result in an eventual activation of the dentate gyrus, whereas we did observe the associative effect of the two stimulations. In all cases the site of stimulation turned out to be in area 36 and LA thus replicating our previous results (Kajiwara et al., 2003). The facilitation of spread of neural activity by two coincident inputs suggest the interaction of the two input pathways. We examined with VSD imaging where in the circuit this interaction between the two pathways is mediated. We hypothesized that if the cortical and amygdala pathways are absolutely independent, the sum of the size of neural event associated with only PC stimulation and that associated with only LA stimulation would be almost equal to the size of neural event associated with the co-stimulation of PC and LA. Our results show this is not the case. That is, a non-linearity is seen over all of the columns. Interestingly, in the deep layer of LEC, the size of neural event associated with the co-stimulation of PC and LA exceeds the sum of the size of neural event associated with only PC stimulation and that associated with only LA stimulation. This means that the association of the two different inputs strengthened the overall excitation in the more medial portions of LEC and even more so in MEC. These findings were taken to indicate that the integration of sensory and emotional inputs is most probably mediated by the circuitry in the deep layer of LEC. Our patch-clamp recordings in the deep layers of LEC are in line with this hypothesis. We showed that there are the cells in the deep layer of LEC that respond to both cortical and amygdala stimulation. Although we made patch-clamp recording on neurons whose shape was apparently pyramidal, we did not identify the class of neurons precisely. The distribution and classification of such cells are now under examination. In view of the fact that we aimed for pyramidal cells, it is quite likely that we included at least a sizable proportion of layer V projection neurons. Although it is well established that EC provides the major source of afferent information to the hippocampus primarily via the superficial layer of EC, via projections from layer II to the dentate gyrus, and CA3 and from layer III to CA1 (Hjorth-Simonsen and Jeune, 1972; Steward and Scoville, 1976; Tamamaki and Nojyo, 1993; Witter, 1993; Witter et al., 1988, 2000), an additional pathway connects the deep layer of the EC (layer V) to the dentate gyrus. The relevance of this connection, although described in both anatomical and electrophysiological studies (Köhler, 1985; Deller et al., 1996; Dugladze et al., 2001; Gloveli et al., 2001), remains obscure. The propagation of neural activity into the dentate gyrus by way of the deep layer of EC as well as the potential for integration of two input pathways in these deep layers as observed in this study indicates the functional relevance of layer V.

It is important to point out that the organization and thus the potential mechanism underlying the observed integration may not be that simple, since in the entorhinal cortex horizontal connections and vertical connections exist both in the superficial layer (layers I–III) and in the deep layer (layers V–VI), such that cells in the superficial and deep layers are functionally interconnected (Köhler, 1986; Lingenhöhl and Finch, 1991; Burwell and Amaral, 1998; Dolorfo and Amaral, 1998; Dugladze et al., 2001; Gloveli et al., 2001; van Haeften et al., 2003). However, the present findings indicate that activation in deep layers of the entorhinal cortex alone is sufficient to activate the dentate gyrus. We therefore suggest that our current functional concept of the entorhinal cortex as

having layers II and III as input layers and layer V as the main output layer is in need for revision.

## References


Barish, M.E., Ichikawa, M., Tominaga, T., Matsumoto, G., Iijima, T., 1996. Enhanced fast synaptic transmission and a delayed depolarization induced by transient potassium current blockade in rat hippocampal slice as studied by optical recording. J. Neurosci. 16, 5672–5687.

Berretta, N., Jones, R.S., 1996. A comparison of spontaneous EPSCs in layer II and layer IV–V neurons of the rat entorhinal cortex in vitro. J. Neurophysiol. 76 (2), 1089–1100.

Burwell, R.D., 2000. The parahippocampal region: corticocortical connectivity. Ann. N. Y. Acad. Sci. 911, 25–42.

Burwell, R.D., Amaral, D.G., 1998. Perirhinal and postrhinal cortices of the rat: interconnectivity and connections with the entorhinal cortex. J. Comp. Neurol. 391, 293–321.

Burwell, R.D., Witter, M.P., 2002. Basic anatomy of the parahippocampal region in monkeys and rats. In: Witter, M.P., Wouterlood, F.G. (Eds.), The Parahippocampal Region, Organisation and Role in Cognitive Functions. Oxford University Press, Oxford, pp. 35–59.

Burwell, R.D., Witter, M.P., Amaral, D.G., 1995. Perirhinal and postrhinal cortices of the rat: a review of neuroanatomical literature and comparison with findings from the monkey brain. Hippocampus 5, 390–408.

Cahill, L., Babinsky, R., Markowitsch, H.J., McGaugh, J.L., 1995. The amygdala and emotional memory. Nature 28, 295–296.

Cahill, L., Haier, R.J., Fallon, J., Alkire, M.T., Tang, C., Keator, D., Wu, J., McGaugh, J.L., 1996. Amygdala activity at encoding correlated with long-term, free recall of emotional information. Proc. Natl. Acad. Sci. U.S.A. 93, 8016–8021.

de Curtis, M., Paré, D., 2004. The rhinal cortices: a wall of inhibition between the neocortex and the hippocampus. Prog. Neurobiol. 74, 101–110.

Deller, T., Martínez, A., Nitsch, R., Frotscher, M., 1996. A novel entorhinal projection to the rat dentate gyrus: direct innervation of proximal dendrites and cell bodies of granule cells and GABAergic neurons. J. Neurosci. 16, 3322–3333.

Dolorfo, C.L., Amaral, D.G., 1998. Entorhinal cortex of the rat: organizations of intrinsic connections. J. Comp. Neurol. 398, 49–82.

Dugladze, T., Heinemann, U., Gloveli, T., 2001. Entorhinal cortex projection cells to the hippocampal formation in vitro. Brain Res. 905, 224–231.

Eichenbaum, H., Yonelinas, A.P., Ranganath, C., 2007. The medial temporal lobe and recognition memory. Annu. Rev. Neurosci. 30, 123–152.

Faulkner, B., Brown, T.H., 1999. Morphology and physiology of neurons in the rat perirhinal–lateral amygdala area. J. Comp. Neurol. 411, 613–642.

Gloveli, T., Dugladze, T., Schmitz, D., Heinemann, U., 2001. Properties of entorhinal cortex deep layer neurons projecting to the rat dentate gyrus. Eur. J. Neurosci. 13, 413–420.

Grinvald, A., Lieke, E.E., Frostig, R.D., Hildesheim, R., 1994. Cortical point-spread function and long-range lateral interactions revealed by real-time optical imaging of macaque monkey primary visual cortex. J. Neurosci. 14, 2545–2568.

Grinvald, A., Manker, A., Segal, M., 1982. Visualization of the spread of electrical activity in rat hippocampal slices by voltage-sensitive optical probes. J. Physiol. 333, 269–291.

Gulyás, A.I., Freund, T.F., 1996. Pyramidal cell dendrites are the primary targets of calbindin D28k-immunoreactive interneurons in the hippocampus. Hippocampus 6, 525–534.

Hamann, S.B., Ely, T.D., Grafton, S.T., Kilts, C.D., 1999. Amygdala activity related to enhanced memory for pleasant and aversive stimuli. Nat. Neurosci. 2, 289–293.

Hjorth-Simonsen, A., Jeune, B., 1972. Origin and termination of the hippocampal perforant path in the rat studied by silver impregnation. J. Comp. Neurol. 144, 215–232.

Iijima, T., Kajiwara, R., Ichikawa, M., Witter, M.P., 1994. Long-lasting neural excitation in the deep layer of perirhinal-cortex is necessary for the propagation of neural activity among the entorhinal–perirhinal–temporal cortices. Soc. Neurosci. Abstr. 20, 800.

Iijima, T., Witter, M.P., Ichikawa, M., Tominaga, T., Kajiwara, R., Matsumoto, G., 1996. Entorhinal–hippocampal interactions revealed by real-time imaging. Science 272, 1176–1179.

Insausti, R., Herrero, M.T., Witter, M.P., 1997. Entorhinal cortex of the rat cytoarchitectonic subdivisions and the origin and distribution of cortical efferents. Hippocampus 7, 146–183.

Kajiwara, R., Takashima, I., Mimura, Y., Witter, M.P., Iijima, T., 2003. Amygdala input promotes spread of excitatory neural activity from perirhinal cortex to the entorhinal–hippocampal circuit. J. Neurophysiol. 89, 2176–2184.

Krettek, J.E., Price, J.L., 1977. The cortical projections of the mediodorsal nucleus and adjacent thalamic nuclei in the rat. J. Comp. Neurol. 171, 157–191.

Köhler, C., 1985. A projection from the deep layers of the entorhinal area to the hippocampal formation in the rat brain. Neurosci. Lett. 56, 13–19.

Köhler, C., 1986. The intrinsic connections of the retrohippocampal region in the rat brain. II. The medial entorhinal area. J. Comp. Neurol. 246, 149–169.

Lingenhöhl, K., Finch, D.M., 1991. Morphological characterization of rat entorhinal neurons in vivo: soma-dendritic structure and axonal domains. Exp. Brain Res. 84, 57–74.

Miettinen, M., Koivisto, E., Riekkinen, P., Miettinen, R., 1996. Coexistence of parvalbumin and GABA in nonpyramidal neurons of the rat entorhinal cortex. Brain Res. 706, 113–122.

Moyer Jr., J.R., Brown, T.H., 1998. Methods for whole-cell recording from visually preselected neurons of perirhinal cortex in brain slices from young and aging rats. J. Neurosci. Methods 86, 35–54.

Murray, E.A., Richmond, B.J., 2001. Role of perirhinal cortex in object perception, memory, and associations. Curr. Opin. Neurobiol. 11, 188–193.

Nishijo, H., Uwano, T., Tamura, R., Ono, T., 1998. Gustatory and multimodal neuronal responses in the amygdala during licking and discrimination of sensory stimuli in awake rats. J. Neurophysiol. 79, 21–36.

Ono, T., Nishijo, H., Uwano, T., 1995. Amygdala role in conditioned associative learning. Prog. Neurobiol. 46, 401–422.

Otsu, Y., Maru, E., Ohata, H., Takashima, I., Kajiwara, R., Iijima, T., 2000. Optical recording study of granule cell activities in the hippocampal dentate gyrus of kainate-treated rats. J. Neurophysiol. 83, 2421–2430.

Paz, R., Pelletier, J.G., Bauer, E.P., Paré, D., 2006. Emotional enhancement of memory via amygdala-driven facilitation of rhinal interactions. Nat. Neurosci. 9, 1321–1329.

Pelletier, J.G., Apergis-Schoute, J., Paré, D., 2005. Interaction between amygdala and neocortical inputs in the perirhinal cortex. J. Neurophysiol. 94, 1837–1848.

Pikkarainen, M., Rönkkö, S., Savander, V., Insausti, R., Pitkänen, A., 1999. Projections from the lateral, basal, and accessory basal nuclei of the amygdala to the hippocampal formation in rat. J. Comp. Neurol. 403, 229–260.

Pinto, A., Fuentes, C., Paré, D., 2006. Feedforward inhibition regulates perirhinal transmission of neocortical inputs to the entorhinal cortex: ultrastructural study in guinea pigs. J. Comp. Neurol. 495, 722–734.

Richardson, M.P., Strange, B.A., Dolan, R.J., 2004. Encoding of emotional memories depends on amygdala and hippocampus and their interactions. Nat. Neurosci. 7, 278–285.

Rosenkranz, J.A., Johnston, D., 2007. State-dependent modulation of amygdala inputs by dopamine-induced enhancement of sodium currents in layer V entorhinal cortex. J. Neurosci. 27, 7054–7069.

Steward, O., Scoville, S.A., 1976. Cells of origin of entorhinal cortical afferents to the hippocampus and fascia dentata of the rat. J. Comp. Neurol. 169, 347–370.

Suzuki, W., Eichenbaum, H., 2000. The Neurophysiology of Memory. New York Academy of Sciences, New York.

Tamamaki, N., Nojyo, Y., 1993. Projection of the entorhinal layer II neurons in the rat as revealed by intracellular pressure-injection of neurobiotin. Hippocampus 3, 471–480.

Tominaga, T., Tominaga, Y., Yamada, H., Matsumoto, G., Ichikawa, M., 2000. Quantification of optical signals with electrophysiological signals in neural activities of Di-4-ANEPPS stained rat hippocampal slices. J. Neurosci. Methods 15, 11–23.

van Haeften, T., Baks-te-Bulte, L., Goede, P., Wouterlood, F.G., Witter, M.P., 2003. Morphological and numerical analysis of synaptic interactions between neurons in the deep and superficial layers of the entorhinal cortex of the rat. Hippocampus 13, 943–952.

von Bohlen und Halbach, O., Albrecht, D., 2002. Reciprocal connections of the hippocampal area CA1, the lateral nucleus of the amygdala and cortical areas in a combined horizontal slice preparation. Neurosci. Res. 44, 91–100.

Witter, M.P., 1993. Organization of the entorhinal–hippocampal system: a review of current anatomical data. Hippocampus 3, 33–44.

Witter, M.P., Amaral, D.G., 2004. The hippocampal formation. In: Paxinos, G. (Ed.), The Rat Nervous System, 3rd ed. Academic Press, San Diego, pp. 635–704.

Witter, M.P., Griffioen, A.W., Jorritsma-Byham, B., Krijnen, J.L.M., 1988. Entorhinal projections to the hippocampal CA1 region in the rat: an underestimated pathway. Neurosci. Lett. 85, 193–198.

Witter, M.P., Wouterlood, F.G., 2002. The Parahippocampal Region. Organization and Role in Cognitive Functions. Oxford University Press, UK.

Witter, M.P., Wouterlood, F.G., Naber, P.A., Van Haeften, T., 2000. Anatomical organization of the parahippocampal-hippocampal network. Ann. N Y Acad. Sci. 911, 1–24.

Wood, S.J., Jones, R.S.G., 1998. Characteristics of spontaneous GABAA receptor-mediated IPSCs in rat entorhinal cortical neurones. J. Physiol. 515, 120.

Woodhall, G.L., Bailey, S.J., Thompson, S.E., Evans, D.I., Jones, R.S., 2005. Fundamental differences in spontaneous synaptic inhibition between deep and superficial layers of the rat entorhinal cortex. Hippocampus 15, 232–245.

Wouterlood, F.G., Van Haeften, T., Eijkhoudt, M., Baks-Te-Bulte, L., Goede, P.H., Witter, M.P., 2004. Input from the presubiculum to dendrites of layer-V neurons of the medial entorhinal cortex of the rat. Brain Res. 1013, 1–12.

nature neuroscience

# A chloride conductance in VGLUT1 underlies maximal glutamate loading into synaptic vesicles

Stephan Schenck[1–3], Sonja M Wojcik[4], Nils Brose[4] & Shigeo Takamori[1–3]

**Uptake of glutamate into synaptic vesicles is mediated by vesicular glutamate transporters (VGLUTs). Although glutamate uptake has been shown to depend critically on $Cl^-$, the precise contribution of this ion to the transport process is unclear. We found that VGLUT1, and not ClC-3 as proposed previously, represents the major $Cl^-$ permeation pathway in synaptic vesicles. Using reconstituted VGLUT1, we found that the biphasic dependence of glutamate transport on extravesicular $Cl^-$ is a result of the permeation of this anion through VGLUT1 itself. Moreover, we observed that high luminal $Cl^-$ concentrations markedly enhanced loading of glutamate by facilitation of membrane potential–driven uptake and discovered a hitherto unrecognized transport mode of VGLUT1. Because a steep $Cl^-$ gradient across the synaptic vesicle membrane exists in endocytosed synaptic vesicles, our results imply that the transport velocity and the final glutamate content are highly influenced, if not determined, by the extracellular $Cl^-$ concentration.**



Intracellular compartments such as endosomes and lysosomes, as well as secretory granules such as chromaffin granules or synaptic vesicles, are energized by the proton-translocating activity of a vacuolar-type $H^+$-ATPase (V-ATPase)[1–4]. The V-ATPase builds up a proton electrochemical gradient ($\Delta\mu H^+$) that is used for transport processes across the membrane. $\Delta\mu H^+$ consists of two components, the membrane potential ($\Delta\Psi$) and the pH gradient ($\Delta$pH), and the ratio of these two components is modulated by the permeability of the membrane for certain ions by leaks or channels[5,6]. Notably, isolated intracellular organelles such as synaptic vesicles acidify only in the presence of small anions such as $Cl^-$ (refs. 5,6). This indicates that $Cl^-$ pathways provide a shunting current for the electrogenic V-ATPase and thereby lead to an increase of $\Delta$pH at the expense of $\Delta\Psi$ by net accumulation of HCl. Regarding the transport of solutes, both $\Delta\Psi$ and $\Delta$pH can be used to energize the translocation process. For instance, biochemical investigations on isolated synaptic vesicles have revealed that the preference for either component depends on the specific transport system for different classical neurotransmitters[7].

Vesicular transport of glutamate, the major excitatory transmitter in the vertebrate brain, is carried out by VGLUTs[8,9] and is believed to be driven primarily by $\Delta\Psi$[10]. A prominent feature of the vesicular glutamate transport is its biphasic dependence on extravesicular $Cl^-$, which has been characterized in biochemical investigations of native synaptic vesicles[11] and in membranes containing heterologous VGLUTs[8,12–15]. The transport activity is very low in the absence of external $Cl^-$, maximal at low concentrations of $Cl^-$ (2–4 mM) and declines with rising $Cl^-$ concentrations from 10–100 mM. Although the decrease in glutamate uptake under conditions of high concentrations of extravesicular $Cl^-$ has been attributed to the increase of $\Delta$pH resulting from a $Cl^-$ channel on synaptic vesicles[10], the very low uptake in the absence of $Cl^-$, despite $\Delta\Psi$ being maximal under these conditions, remains largely unexplainable. The transport of glutamate was therefore believed to be activated in the presence of low millimolar concentrations of $Cl^-$ by regulatory binding of this ion to the transporter itself[16]. However, there are also indications for a role of the luminal pH, which could explain the activation of transport by low concentrations of $Cl^-$ (ref. 17). Because the ratio of $\Delta\Psi$ and $\Delta$pH profoundly influences the uptake of glutamate and other transmitters, the molecular signature of the $Cl^-$ channel is crucial for understanding the loading process and its regulation. Despite some progress[6], the underlying $Cl^-$ shunt in synaptic vesicles has remained elusive for a long time.

ClC-3, a member of the CLC gene family, has been an attractive candidate for $Cl^-$ shunting on synaptic vesicles because the acidification of synaptic vesicles derived from *Clcn3*$^{-/-}$ mice is partially impaired[18]. However, the loss of ClC-3 does not cause major changes in neurotransmission and vesicular glutamate transport of isolated vesicles retains its biphasic dependence on $Cl^-$ even in the absence of ClC-3 (ref. 18). This is surprising, as the loss of a $Cl^-$ shunt would be expected to influence $\Delta$pH and, consequently, glutamate loading. Recently, indications for a $Cl^-/H^+$ exchange have been found for ClC-3 (ref. 19). This has already been demonstrated for ClCec1 (a bacterial homolog of eukaryotic ClCs)[20], ClC-4/5 (refs. 21,22) and ClC-7 (ref. 23). The $Cl^-/H^+$ exchange mechanism does not exclude a role for ClC-3 in acidification. However, it nevertheless complicates the interplay with a proton pump, and together with the pronounced outward rectification of intracellular ClCs[19,24], the observed co-transport of $Cl^-$ and $H^+$ in isolated synaptic vesicles cannot be well explained.

[1]Center for Brain Integration Research, [2]21st Century Center of Excellence Program, [3]Department of Neurology and Neurological Sciences, Graduate School of Medicine, Tokyo Medical and Dental University, 1-5-45 Yushima, Bunkyo-ku, Tokyo 113-8519, Japan. [4]Department of Molecular Neurobiology, Max-Planck-Institute for Experimental Medicine, Hermann-Rein-Strasse 3, D-37075 Göttingen, Germany. Correspondence should be addressed to S.T. (taknuro@tmd.ac.jp).

Received 22 July 2008; accepted 2 December 2008; published online 25 January 2009; doi:10.1038/nn.2248

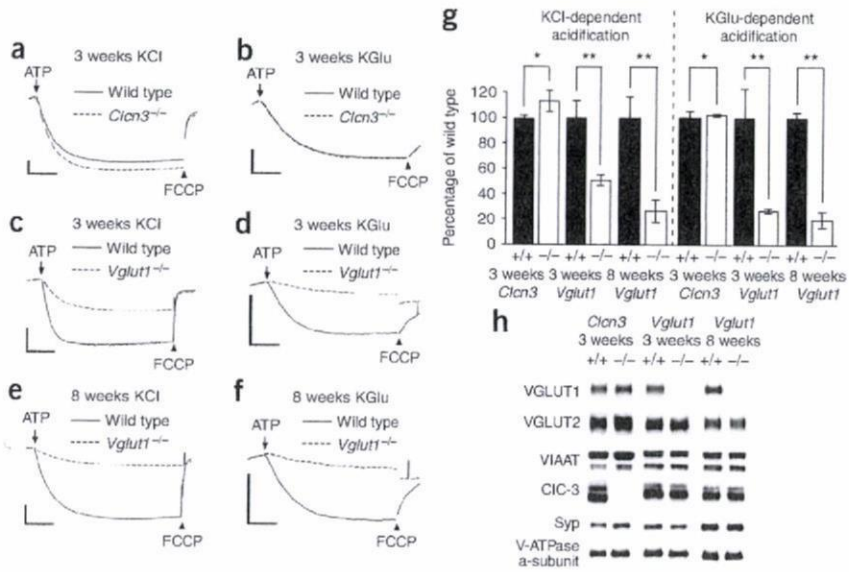


**Figure 1** Acidification of synaptic vesicles from *Clcn3*$^{-/-}$ and *Vglut1*$^{-/-}$ brains in the presence of external $Cl^-$ or glutamate. (**a**,**b**) Acidification of synaptic vesicles from wild-type and *Clcn3*$^{-/-}$ mice at the age of 3 weeks in the presence of 100 mM KCl (**a**) or 4 mM KCl + 10 mM potassium glutamate (KGlu) (**b**) measured under standard conditions (see Methods). A decrease in fluorescence reflects acidification. (**c**–**f**) $Cl^-$- and glutamate-dependent acidification of synaptic vesicles from wild-type and *Vglut1*$^{-/-}$ mice at the age of 3 (**c**,**d**) and 8 weeks (**e**,**f**) was measured as described in **a** and **b**. Scale bars for all traces represent 500 AU and 120 s. (**g**) Quantitative summary of the extent of acidification for *Clcn3*$^{-/-}$ and *Vglut1*$^{-/-}$ samples compared with wild-type samples (from **a**–**f**). Data were quantified as described in Methods and analyzed with two-tailed unpaired *t* test (* $P > 0.1$, ** $P < 0.05$). (**h**) Representative immunoblots of relevant proteins in the synaptic vesicle fractions from *Clcn3*$^{-/-}$ and *Vglut1*$^{-/-}$ mice compared with wild type. Syp, synaptophysin. Error bars represent s.d.

Notably, the loss of ClC-3 is accompanied by a decrease of the VGLUT1 content in synaptic vesicle fractions and of glutamate uptake into synaptic vesicles[18], presumably as a result of neurodegeneration, including the complete loss of hippocampus. VGLUT1, in turn, has been shown to induce a $Cl^-$ conductance when heterologously expressed, which can be inhibited by glutamate[8]. This is a strong indication for a $Cl^-$ conductance in the transporter itself. These observations cast doubts on whether the observed partial reduction in $Cl^-$-dependent acidification in synaptic vesicles from *Clcn3*$^{-/-}$ brains is caused by the loss of ClC-3, but suggest that it is an indirect effect linked to the reduction of VGLUT1. In view of the biphasic dependence of glutamate transport on extravesicular $Cl^-$ and the indications for direct binding of $Cl^-$ (ref. 16), there is a clear need to elucidate the contribution of VGLUT1 in this context and to unmask the molecular identity of the $Cl^-$ translocator on synaptic vesicles to gain a correct understanding of glutamate loading.

## RESULTS

### Impaired synaptic vesicle acidification in *Vglut1*$^{-/-}$ mice

To clarify the contribution of either ClC-3 or VGLUT1 on the anion conductance of synaptic vesicles, we prepared synaptic vesicle fractions from the brains of mice lacking ClC-3 or VGLUT1 (refs. 25,26) and analyzed ATP-dependent acidification using acridine orange fluorescence quenching (see Methods) (**Fig. 1**). The previous investigation of synaptic vesicle fractions from *Clcn3*$^{-/-}$ mice was carried out with material obtained from adult mice after severe neurodegeneration had affected the brain, including the complete loss of the hippocampus[18]. To rule out possible bias resulting from neurodegeneration, we sought to isolate vesicles from *Clcn3*$^{-/-}$ brains before the onset of degeneration at the age of 3 weeks. In contrast with the former data from adult brains, we did not detect any signs of reduction of either $Cl^-$- or glutamate-dependent acidification in knockout samples (**Fig. 1a**,**b**,**g**). Notably, we did not detect a reduction in the VGLUT1 content (**Fig. 1h** and **Supplementary Fig. 1** online), which also differed from previously published data. Furthermore, we estimated the copy number of ClC-3 per vesicle to be approximately 0.001 ClC-3 per synaptic vesicle (only every 2,000$^{th}$ synaptic vesicle may thus bear a functional dimer), making a contribution of ClC-3 as a $Cl^-$ translocator on bulk synaptic vesicles very unlikely (**Supplementary Fig. 2** online).

In contrast, synaptic vesicle fractions from *Vglut1*$^{-/-}$ (also known as *Slc17a7*) mice showed a strong reduction in both $Cl^-$- and glutamate-dependent acidification at the age of 3 (**Fig. 1c**,**d**,**g**) and 8 weeks (**Fig. 1e**–**g**). There were no major changes in the expression levels of relevant synaptic proteins; in particular, there was no reduction on the ClC-3 content (**Fig. 1h** and **Supplementary Fig. 1**). The remaining acidification in the *Vglut1*$^{-/-}$ samples can be well explained with the fractional content of synaptic vesicles that are positive for VGLUT2 and the vesicular inhibitory amino acid transporter (VIAAT), which presumably also bear a $Cl^-$-translocating factor[27,28]. Taken together, the comparison of the two knockout strains favored the idea that VGLUT1 is serving as a $Cl^-$ shunt on a major fraction of synaptic vesicles (approximately 65%)[28].

### Purified VGLUT1 shows a $Cl^-$ conductance

To verify that the $Cl^-$ conductance is indeed an intrinsic property of VGLUT1, we attempted to purify the transporter (**Fig. 2**). We were able to obtain a pure preparation of recombinant rat VGLUT1 from tsA201 cells (see Methods; **Fig. 2a**). The transporter was efficiently reconstituted into membranes, eluted as a single peak without signs of aggregation in analytical gel filtration (data not shown) and showed biological activity as described below. We used a bacterial ATP synthase ($TF_0F_1$)[29] (**Fig. 2a**) to energize reconstituted liposomes, which acidified in symmetric potassium gluconate solution only when free counter-ion movement was made possible by addition of the $K^+$ ionophore valinomycin (VAL; **Fig. 2b**). The electrogenic properties of this $TF_0F_1$ preparation resemble the V-ATPase[2] and are therefore suitable for examining the conductance in VGLUT1. Co-reconstitution of VGLUT1 and $TF_0F_1$ into liposomes revealed a conductance for $Cl^-$ in VGLUT1 (**Fig. 2d**,**e**), as evident from acidification, but not for a bulky anion such as gluconate or a cation such as $K^+$ (**Fig. 2d**,**e**). Similar results were seen when we replaced internal gluconate with acetate or $Cl^-$ (data not shown). Control liposomes bearing only $TF_0F_1$ did not acidify when external $Cl^-$ was present (**Fig. 2c**,**e**).

When we reconstituted increasing amounts of VGLUT1 and measured the acidification depending on $Cl^-$ and in $Cl^-$-free medium by the addition of VAL (**Fig. 2f**), we found that reconstitution of VGLUT1 did not affect the properties of the liposomes, except for the introduced $Cl^-$ conductance. We further ruled out major contaminations as a

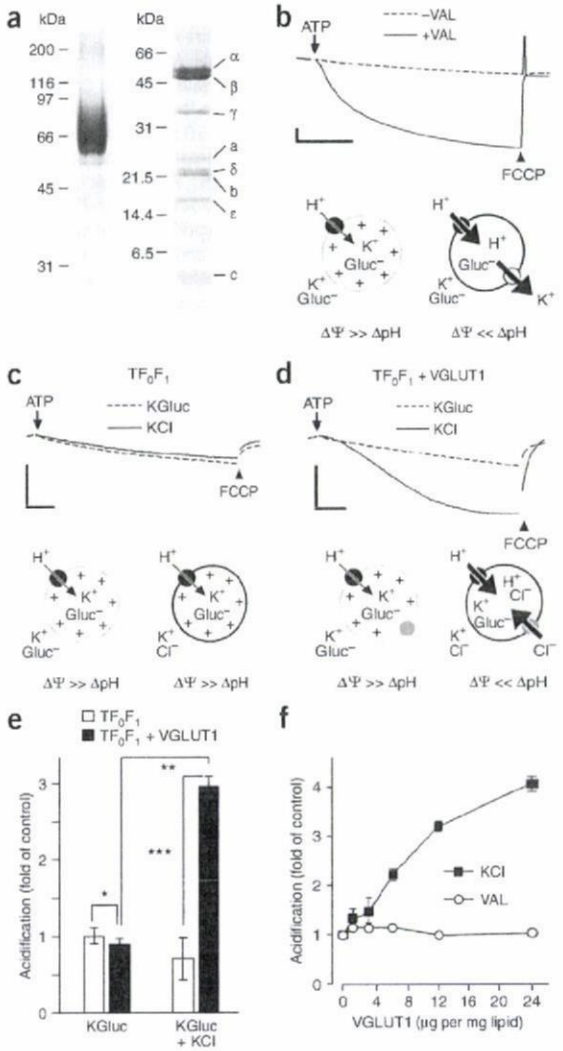


**Figure 2** Purified VGLUT1 shows a $Cl^-$ conductance. (**a**) Coomassie blue staining of recombinant rVGLUT1 (18 μg, 10% SDS-PAGE, left) and $TF_0F_1$ (10 μg, 15% SDS-PAGE, right). (**b**) Electrogenic properties of reconstituted $TF_0F_1$ (5 μg). Efficient proton coupling appeared only in the presence of the $K^+$-ionophore VAL as measured by fluorescence quenching of acridine orange. Representative traces are shown. The sketch below illustrates ion movements. $TF_0F_1$ is represented by black filled circles and VAL by an open circle. The strength of $\Delta\Psi$ is symbolized by + and low pH by $H^+$. (**c**) Acidification in control liposomes containing only $TF_0F_1$ in the presence of gluconate (dashed line) or $Cl^-$ (solid line). (**d**) Acidification in liposomes co-reconstituted with $TF_0F_1$ and VGLUT1 in the presence of external gluconate (dashed line) or $Cl^-$ (solid line). Sketches are labeled as in **b**. The gray circle symbolizes VGLUT1. (**e**) Quantitative summary of the traces in **c** and **d** normalized to the acidification of $TF_0F_1$ liposomes in symmetric potassium gluconate buffer (control). Data were analyzed with two-tailed paired (** $P < 0.001$) and two-tailed unpaired *t*-tests (* $P > 0.3$, *** $P < 0.005$). (**f**) $Cl^-$ influx was VGLUT1 dose dependent, as shown by increasing concentrations of VGLUT1. The VAL-dependent acidification (single measurements) was not affected. Values are normalized to the mean acidification of $TF_0F_1$-liposomes without VGLUT1 in the presence of 100 mM external KCl (filled squares) or 100 mM symmetric potassium gluconate buffer containing VAL (open circles). All scale bars represent 500 AU and 120 s. Data were quantified as described in Methods. Error bars represent s.d.



source of the observations to verify that the $Cl^-$ conductance arose from VGLUT1 by removing the transporter from the liposome premix with an affinity purified antibody (**Supplementary Fig. 3** online).

### Intravesicular $Cl^-$ strongly increases glutamate uptake

Having verified that VGLUT1 is responsible for both glutamate transport and $Cl^-$ permeability in liposomes and synaptic vesicles, we attempted to test in detail how the $Cl^-$ conductance in VGLUT1 influences glutamate transport. To date, only the effects of extravesicular $Cl^-$ could be investigated using native vesicles and those of intravesicular $Cl^-$ have never been examined experimentally, to the best of our knowledge. However, synaptic vesicles engulf extracellular fluid during endocytosis and should therefore be filled with ~130 mM NaCl. Thus, we preloaded liposomes with 100 mM KCl or 100 mM potassium gluconate and measured glutamate uptake in the presence of 4 mM external $Cl^-$, which is known to be optimal for uptake[11,17] (see **Fig. 3a** for an illustration of $Cl^-$ and gluconate distributions). Notably, the ATP-dependent uptake of glutamate was strongly enhanced in the presence of luminal $Cl^-$ compared with impermeable gluconate approximately threefold (**Fig. 3b**).

A time course of glutamate uptake indicated an increased velocity as well as a higher loading capacity (**Fig. 3c**). The uptake kinetics revealed a substantial increase in $v_{max}$ (3.3-fold), whereas the affinities measured for both gluconate- and $Cl^-$-loaded liposomes differed only slightly and approximated previously reported values ($K_M$ ~1–2 mM[11,30]; **Fig. 3d,e**).

### External $Cl^-$ modulates glutamate uptake into liposomes

To investigate whether the biphasic dependence of glutamate transport on extravesicular $Cl^-$ is preserved in our minimal system and can be explained by the conductance in VGLUT1, we measured glutamate uptake in the presence of different external $Cl^-$ concentrations for both of the tested internal anions (**Fig. 4a–c**). Notably, the dependence on external $Cl^-$ for gluconate-loaded liposomes resembled the pattern that was observed for isolated synaptic vesicles[11,17], where the uptake was very low in the absence of external $Cl^-$, was enhanced by low millimolar $Cl^-$ (~6-fold) and was attenuated by rising external $Cl^-$ concentrations (**Fig. 4b,c**). $Cl^-$-loaded liposomes also showed enhanced uptake at low millimolar concentrations of $Cl^-$, albeit weaker (~1.2-fold) than that observed for gluconate-loaded liposomes, and uptake was attenuated by rising external $Cl^-$ concentrations in a similar manner (**Fig. 4b,c**). In the absence of external $Cl^-$, however, the uptake by $Cl^-$-loaded liposomes was about tenfold higher than that of gluconate-loaded liposomes ($[Cl^-]_{out} = 0$; **Fig. 4b,c**).

For all the conditions tested, we essentially observed a higher uptake for the $Cl^-$-loaded liposomes than for the gluconate-loaded liposomes, but this was most obvious under conditions with high $\Delta\Psi$. For uptake with close to physiologically relevant concentrations of glutamate (5 mM), the difference in uptake between the two tested anions was even bigger (**Fig. 4c**).

### Intravesicular $Cl^-$ facilitates $\Delta\Psi$-driven glutamate uptake

To evaluate the role of protons in the transport process, we used the $K^+/H^+$ exchanger nigericin (NIG), which selectively dissipates ΔpH. This allowed us to estimate the relative contributions of either $\Delta\Psi$ or ΔpH on the net uptake of glutamate into liposomes (**Fig. 4b,c**). The NIG-resistant uptake, driven by $\Delta\Psi$, was much larger if the liposomes were loaded with $Cl^-$, maximal in the absence of external $Cl^-$ and gradually decreased with raising external $Cl^-$ concentrations. In contrast, the transport driven by $\Delta\Psi$ into gluconate-loaded liposomes was very low, although minimal uptake at low millimolar concentrations of

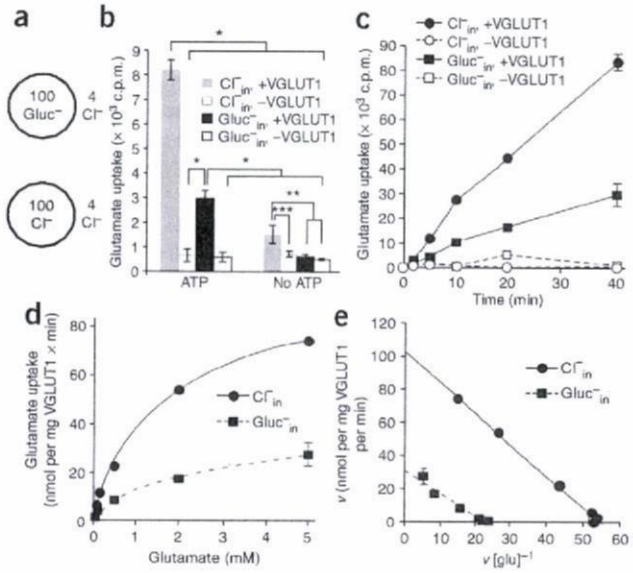


**Figure 3** Enhancement of glutamate transport into liposomes by high luminal $Cl^-$ concentrations. (**a**) Sketch showing the internal and external concentrations of $Cl^-$ and gluconate of liposomes used for experiments in this figure in mM. (**b**) Glutamate uptake (12 min) into liposomes preloaded with potassium gluconate (black) and KCl (gray) under standard conditions (see Methods) with or without the addition of ATP. Uptake into liposomes lacking VGLUT1 is shown in open bars. * $P < 0.01$, ** $P < 0.05$ and *** $P = 0.053$ (two-tailed unpaired $t$ tests). (**c**) Time course of glutamate uptake into liposomes preloaded with potassium gluconate (squares) and KCl (circles) under standard conditions. Uptake into liposomes lacking VGLUT1 is shown in the traces with dashed lines (single measurements). (**d**) Kinetics of glutamate uptake under standard conditions with liposomes preloaded with KCl (solid line) and potassium gluconate (dashed line), respectively. Data were taken after 15 min uptake with varying concentrations of nonlabeled glutamate. (**e**) Eadie-Hofstee plot of the data in **d**. $K_M$ (mM) and $v_{max}$ (nmol glutamate per mg VGLUT1 per min) were 1.36 ± 0.19 and 23.41 ± 3.32 for gluconate-loaded liposomes and 1.86 ± 0.03 ($P < 0.05$) and 76.89 ± 1.7 ($P < 0.0005$) for $Cl^-$-loaded liposomes, respectively (independent two-tailed $t$ tests). Error bars represent s.d.

external $Cl^-$ remained. Clearly, $\Delta\Psi$-driven transport of glutamate is only possible when $Cl^-$ is present in the lumen. Uptake for gluconate-loaded liposomes appeared to be entirely fueled by $\Delta$pH, indicating an $H^+$/glutamate antiport. It should be noted that this component is also present in $Cl^-$-loaded liposomes and contributes to the total uptake. An additional conclusion that can be drawn from the effect of NIG is that high external $Cl^-$ concentrations do not necessarily reduce uptake by imposing a larger $\Delta$pH, as this component must be negligible in the presence of the ionophore. This can be seen for $Cl^-$-loaded liposomes (**Fig. 4b,c**) and indicates competition of $Cl^-$ with glutamate for entering the lumen.

We further characterized the uptake of $Cl^-$-loaded liposomes in the absence of external $Cl^-$, which demonstrated its marked dependence on the membrane potential. Dissipation of $\Delta\Psi$ by application of VAL abolished the transport (**Fig. 4d**). The transport was consequently strongly reduced by dissipation of $\Delta\mu H^+$ (NIG + VAL and carbonyl cyanide *p*-(trifluoromethoxy)phenylhydrazone (FCCP); **Fig. 4d**). We observed a strict dependence on the actual internal $Cl^-$ concentration (**Fig. 4e**), which indicates that $Cl^-$ is a substrate during the transport. Alternatively, the inside positive membrane potential generated by leaking $Cl^-$ through VGLUT1 could also contribute to the driving force. It might explain the slightly elevated uptake in the absence of ATP when compared with gluconate-loaded liposomes (**Fig. 3b**), but generation of $\Delta\Psi$ by $TF_0F_1$ is essential, probably by inducing conformational changes in the transporter that are necessary for substrate translocation[30].

Uptake was inhibited by 1 μM Evan's Blue, a known inhibitor of vesicular glutamate transport[31], by approximately 60% (**Fig. 4f**), but $Cl^-$-dependent acidification was not affected at the same concentration (**Fig. 4g**). This supports the view of two independent binding sites for glutamate and $Cl^-$ on the transporter[16], but it does not exclude a possible overlap.

In summary, liposomes preloaded with either gluconate or $Cl^-$ clearly showed distinct biophysical characteristics. Therefore,

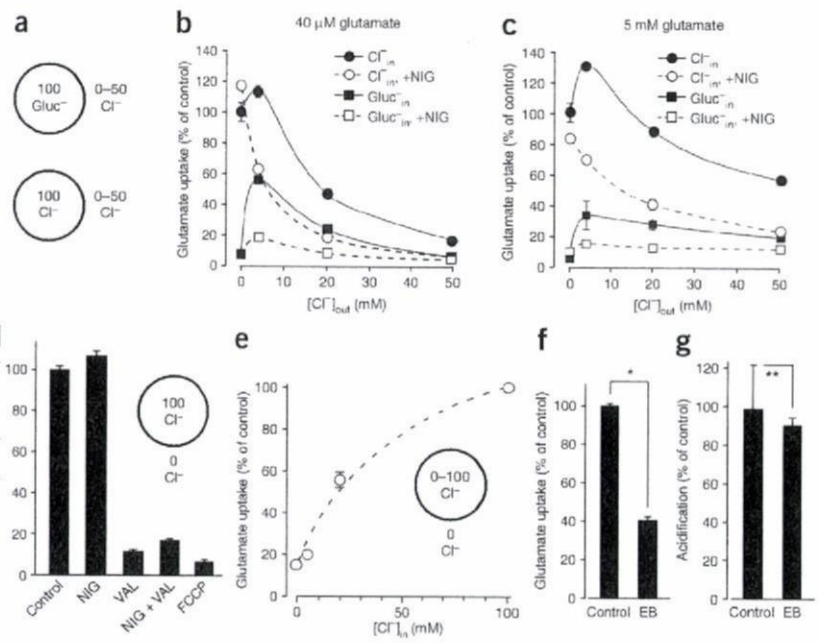


**Figure 4** Dependence of glutamate transport on extravesicular $Cl^-$ and contribution of $\Delta$pH and $\Delta\Psi$ on the total uptake. (**a**) Sketch showing the internal and external concentrations of $Cl^-$ and gluconate of liposomes used for experiments in **b** and **c** in mM. (**b**,**c**) Glutamate uptake (30 min) into liposomes containing potassium gluconate (squares) and KCl (circles) under varying external $Cl^-$ concentrations in the absence (solid lines) and presence of NIG (dashed lines). Uptake with either 40 μM glutamate (**b**) or 5 mM glutamate (**c**) was assayed. The data were normalized to a control (100 mM $Cl^-_{in}$, 0 mM $Cl^-_{out}$, no NIG). (**d**) Glutamate uptake in the presence of different ionophores (see Methods). The data were normalized to a control (transport without any additives). (**e**) Glutamate uptake under varying internal $Cl^-$ concentrations without external $Cl^-$. Data in the presence of 100 mM internal $Cl^-$ were taken as 100%. (**f**) Effect of 1 μM Evan's Blue (EB) on glutamate transport (100 mM $Cl^-_{in}$, 0 mM $Cl^-_{out}$) after 30 min uptake. (**g**) Effect of 1 μM EB on the acidification of liposomes. Data in **f** and **g** was analyzed with two-tailed paired $t$ tests (* $P < 0.001$, ** $P > 0.5$). Error bars represent s.d.

slight differences in the volume of liposomes formed in potassium gluconate– or KCl-based buffers are very unlikely to explain our observations (**Supplementary Fig. 4** online).

## DISCUSSION

Departing from uncertainties and unresolved issues concerning the $Cl^-$ conductance on synaptic vesicles, we found clear indications that VGLUT1 (and probably VGLUT2 as well) underlies the $Cl^-$ conductance of a major fraction of synaptic vesicles by analyzing the acidification in synaptic vesicles of mice lacking this transporter. We further validated this conductance in a reconstituted system of minimal complexity. As the conductance and the glutamate transport activity arise from the same protein, all further experiments can be interpreted with this in mind. Notably, we observed a biphasic dependence of uptake on the extravesicular $Cl^-$ concentration in our reconstituted system, which strongly indicates that previous observations on synaptic vesicles are also based on only two components, the V-ATPase and VGLUT. This makes an additional $Cl^-$ channel for VGLUT-positive vesicles obsolete, although we cannot exclude its existence with certainty (VGLUT1/2-positive synaptic vesicles comprise ~80% of all synaptic vesicles[28]). However, the most important finding is represented by the strong enhancement of glutamate transport by luminal $Cl^-$, a condition that was experimentally inaccessible before reconstitution of purified components.

In summary, our observations allow for a number of conclusions about the glutamate-loading mechanism of synaptic vesicles. First, VGLUT1 efficiently transports glutamate solely driven by $\Delta\Psi$, but to do so a charge-compensating exchange with a luminal anion is necessary. $Cl^-$ serves this role and the $Cl^-$ permeation pathway is provided by VGLUT1 itself (**Supplementary Fig. 5** online). If a permeable internal anion is missing, the $\Delta\Psi$-driven transport is extremely low. Second, when external $Cl^-$ is present, part of the transport will depend on $\Delta$pH and therefore be sensitive to NIG (**Fig. 4b,c** and **Supplementary Fig. 5**). Again, this can be attributed to the $Cl^-$ conductance in VGLUT1, as only VGLUT1 can provide a shunting current that would lead to an increase of $\Delta$pH in our reconstituted system. Apparently, VGLUT1 can operate also as an $H^+$/glutamate exchanger and, if no permeable anion is present on the luminal side, will transport glutamate almost entirely in this fashion, as the remaining NIG-insensitive component was very small (**Fig. 4b,c**). Finally, low millimolar concentrations of extravesicular $Cl^-$ do not activate transport by regulatory binding to VGLUT1, contrary to previous interpretations[16,32,33]. When the $\Delta$pH component was abolished by NIG, glutamate uptake was reduced also at low extravesicular $Cl^-$ concentrations (**Fig. 4b,c**). This effect was stronger when glutamate concentrations were low, pointing to the competitive character of $Cl^-$. Consequently, high external $Cl^-$ concentrations reduce the uptake further, as $Cl^-$ is competing with glutamate for $\Delta\Psi$-driven entry and/or occupies the transporter in a certain conformational state.

Because synaptic vesicles are loaded with ~100 mM glutamate[34], it appears more likely that the bigger portion of the uptake in synaptic vesicles is driven by $\Delta\Psi$, as the $H^+$/glutamate exchange is restricted by osmotic barriers and would require swelling of synaptic vesicles. Storage of glutamate as a free acid in synaptic vesicles would result in a very low pH of 3–3.5, over two pH units lower than reported values[35], and the luminal osmolality would reach values of 400–500 mOsm, which are unlikely to persist in synaptic vesicles. The only way to evade this physical barrier is the efflux of other osmolytes, as there is no evidence for a transmitter-storing matrix in glutamate-filled synaptic vesicles[28]. In a scenario where $Cl^-$ is extruded in parallel with glutamate uptake (**Supplementary Fig. 5**), the transmitter would be stored mainly as sodium glutamate, thus overcoming the drop of pH, insolubility and osmotic imbalance, as proposed earlier[36]. It also explains why the uptake that is usually assayed in isolated synaptic vesicles under maximal $\Delta\Psi$ is very low and resembles the uptake that we observed in gluconate-loaded liposomes. Isolated synaptic vesicles must have lost most of the luminal $Cl^-$ during the glutamate loading process (**Supplementary Fig. 5**).

Indications for the exchange of $Cl^-$ and glutamate have also been obtained with native vesicles, which led to the proposal of an antiporter model[30]. When synaptic vesicles were preloaded with glutamate and $\Delta$pH was clamped, application of $Cl^-$ in relatively high concentrations to the assay medium induced efflux of glutamate. Our data are largely compatible with this model. However, VGLUT1 translocates $Cl^-$ even in the absence of glutamate and $\Delta$pH can also be used for the uptake. Currently, we cannot clearly distinguish whether influx and efflux of $Cl^-$ are mediated by the same mechanism in VGLUT1.

Some recent experiments aimed to influence the glutamate content of synaptic vesicles by raising the cytosolic $Cl^-$ concentration above normal levels[37,38], as this could be predicted by the long-known biphasic dependence on extravesicular $Cl^-$ (refs. 11,17). On the basis of our data, however, we would expect a net influx of HCl into synaptic vesicles rather than a glutamate efflux from already charged vesicles. Future investigations might resolve some of these issues in more detail, but must also confirm turnover of synaptic vesicles to see changes in the dynamics of vesicle loading.

VGLUTs have been proposed to be involved in the determination and regulation of quantal size[7,39]. This has been mainly addressed to their copy number[26,40,41] or to changes in vesicle size[40] and critically depends on the filling model applied for synaptic vesicles[7]. The transport mode described here is therefore an important factor to consider in this context. Although we cannot provide experimental evidence for it, the $Cl^-$ content of freshly endocytosed synaptic vesicles would be a major determinant for the total glutamate load. If the extracellular $Cl^-$ concentration is the limiting factor, the size of quanta in these terminals can be expected to be very stable. In addition, the reloading kinetics of synaptic vesicles with glutamate should be closely linked to the initial intravesicular $Cl^-$ concentration just after endocytosis. Because the loading of synaptic vesicles with glutamate is potentially a limiting step in neurotransmission when rapidly recycling synaptic vesicles are involved, the utilization of intravesicular $Cl^-$ in the translocation process could be a means to ensure fast reloading and therefore stable quantal size during prolonged high release rates. However, this assumption has to be confirmed experimentally; for example, by replacing extracellular $Cl^-$ with an impermeable anion under conditions that ensure turnover of synaptic vesicles in all pools in the necessary dimensions.

## METHODS

**Synaptic vesicle preparations.** Crude synaptic vesicle fractions (LP2) were isolated as described[42], adjusted to 2.5 mg of protein per ml and stored at –80 °C. Acidification was measured with 20–60 µg LP2 by acridine orange quenching in 1 ml of assay buffer (0.3 M sucrose, 4 mM $MgSO_4$, 2 µM acridine orange, 10 mM MOPS, pH 7.3) in a Hitachi F2500 fluorometer (excitation, 492 nm, emission, 530 nm) at 32 °C. ATP (4 mM) and FCCP (40 µM) were added as indicated. For $Cl^-$-dependent acidification, KCl was added to final concentrations of 100 mM, and for glutamate-dependent acidification, KCl and potassium glutamate were added to reach 4 mM and 10 mM, respectively. Measurements were quantified by taking the difference in fluorescence 10 s after ATP mixing and 10 s before FCCP addition. Traces were normalized to the fluorescence at $t = 0$. The rapid increase of acridine orange-fluorescence caused by the addition of ATP was subtracted. LP2 fractions were obtained

from 5–12 mice. In one preparation, equal numbers of animals were used, and two independent preparations for each developmental stage were made to verify the observations.

**Antibodies.** The rabbit polyclonal antisera to VGLUT1, VGLUT2, VIAAT, V-ATPase a-subunit (pp116) and GFP that we used were a kind gift from R. Jahn (Max-Planck-Institute for Biophysical Chemistry) and are commercially available from Synaptic Systems GmbH. VGLUT1, VGLUT2 and VIAAT antibodies were affinity purified with the corresponding antigens. Synaptophysin was detected with the mouse monoclonal antibody Cl 7.2 (Synaptic Systems) and also donated by R. Jahn. Guinea pig antibody to VGLUT1 (ref. 43) was a kind gift of T. Kaneko (University of Kyoto). The affinity-purified rabbit polyclonal antibody-to rClC-3 came from Alomone Labs.

**DNA constructs.** The entire open reading frame of rat VGLUT1 was cloned into pcDNA3.1 (Invitrogen), N-terminally connected to the streptavidin binding–peptide tag by a TEV-linker. The streptavidin binding–peptide tag was amplified by PCR from the plasmid pTAG2K[44]. The 5′-UTR of human VEGF (PCR amplified from pcDNA4-Hismax, Invitrogen) was positioned upstream of the start codon. Rat VGLUT1 and hClC3 (a kind gift of T.J. Jentsch, Leibniz-Institut), C-terminally fused to Venus (a kind gift of A. Miyawaki, BSI-RIKEN) and EGFP (Clontech), respectively, were cloned into pcDNA3.1. All constructs were verified by Sanger sequencing.

**Protein purification.** VGLUT1 was heterologously expressed in tsA201 cells and purified in a single step with streptavidin beads. The cells were grown in DMEM with 4.5 g $l^{-1}$ glucose, supplemented with 2 mM L-glutamine, 1 mM sodium pyruvate, 50 U $ml^{-1}$ penicillin, 50 μg $ml^{-1}$ streptomycin (all from Sigma) and 10% FBS (vol/vol) under 5% $CO_2$. For expression, typically 100 10-cm dishes of cells at 60–70% confluency were transfected with 2 mg of plasmid DNA (Maxi Prep, Macherey-Nagel) by the calcium-phosphate method[45]. After overnight transfection with $CO_2$ set to 2.8%, the medium was changed and expression was continued for 24 h under 5% $CO_2$, until the cells were harvested by centrifugation. The pellets were resuspended in 80 ml of ice-cold Buffer A (300 mM KCl, 40 mM Tris-Cl and 2 mM EDTA, pH 7.5). Cells were lysed after addition of β-mercaptoethanol (5 mM final), PMSF (1 mM final) and solid n-dodecyl-β-D-maltopyranoside (DDM) (2% wt/vol final) at 4 °C for 30 min under stirring. The lysate was cleared for 20 min by centrifugation (300,000 *g*, 4 °C). After additional ultrafiltration, the clear supernatant was incubated in batch with ~1 ml of streptavidin beads (UltraLink, Pierce) for 3 h at 4 °C. The beads were washed with 20 bed volumes of ice-cold Buffer A supplemented with 5 mM β-mercaptoethanol and 0.08% DDM (wt/vol). For elution, 1 ml of elution buffer (100 mM KCl, 13 mM Tris-Cl, 0.6 mM EDTA, 2 mM (+)-biotin, 5 mM β-mercaptoethanol and 0.04% DDM (wt/vol), pH 7.4) was incubated with the beads for 10 min on ice for five cycles. The supernatants were pooled and concentrated with Amicon Spin concentrators (50-kDa cutoff, Millipore) to approximately 1 mg $ml^{-1}$ VGLUT1 and 1% DDM. Purified VGLUT1 was frozen in liquid nitrogen and stored at –80 °C. We regularly obtained yields of 200–400 μg VGLUT1.

His-tagged ATP synthase holoenzyme ($TF_0F_1$) from the thermophilic *Bacillus sp.* PS3 was constitutively expressed in *E. coli* DK8 (native *unc* operon deleted) from the plasmid pTR19ASDS[29]. Cells were grown to an $OD_{600}$ of 1.5–2 in the presence of 100 μg of ampicillin per ml in 2 l TB medium. After harvesting by centrifugation, the pellet was resuspended in 50 mM Tris-Cl, 0.5 mM EDTA and 1 mg $ml^{-1}$ lysozyme at pH 8.0, and incubated at 37 °C for 1 h. After the addition of $MgCl_2$ (5 mM final), the suspension was sonicated for 2 min on ice. DNase I, $Na_2SO_4$ and sodium cholate were added to reach final concentrations of 1 μg $ml^{-1}$, 250 mM and 0.7% (wt/vol), respectively. The suspension was stirred for 20 min at 25 °C and centrifuged at 20,000 *g* at 4 °C. The washed pellet was resuspended in Buffer C (100 mM KCl, 20 mM imidazole, 5 mM $MgCl_2$ and 1% DDM (wt/vol), pH 7.6), stirred at 25 °C for 45 min and centrifuged with 20,000 *g* at 4 °C. The supernatant was batch incubated with Talon beads (Clontech) for 2 h at 25 °C and washed with ten column volumes of Buffer C, but with DDM reduced to 0.08% (wt/vol). Elution of the protein complex was achieved with 250 mM imidazole, 50 mM KCl, 5 mM $MgCl_2$ and 0.05% DDM (wt/vol), which was then dialyzed at 25 °C against 20 mM NaCl, 20 mM HEPES and 5 mM $MgCl_2$, pH 7.5. The sample was concentrated using a MonoQ column and subsequently eluted from a Superdex 200 column using an ÄKTA System (GE) in 100 mM KCl, 10 mM HEPES, 5 mM $MgCl_2$ and 0.05% DDM (wt/vol), pH 7.4. Yields of 10 mg were obtained and $TF_0F_1$ was stable at 4 °C for several weeks.

**Proteoliposomes.** For reconstitution, soybean phospholipids (type II from Sigma, 40 mg $ml^{-1}$ in 7% n-octyl-β-D-glucopyranoside) were mixed with cholesterol (Wako, 5 mg $ml^{-1}$ in 7% n-octyl-β-D-glucopyranoside) to a cholesterol content of ~25% (mol/mol) and proteins were subsequently added. Lipids and proteins were mixed at a ratio (wt/wt) of ~50 for $TF_0F_1$ and ~25 for VGLUT1. A final lipid concentration of 2.5 mg $ml^{-1}$ was kept by adjusting with buffer. When VGLUT1 was omitted, the corresponding elution buffer containing 1% DDM was added instead. Liposomes were formed by dialysis in 5 mM MOPS (pH 7.3) containing 2 mM $MgSO_4$ and either 100 mM potassium gluconate or 100 mM KCl at 4 °C for 12 h. Intermediate $Cl^-$ concentrations were achieved by mixing potassium gluconate– and KCl-based buffers accordingly. After dialysis, DDM was complexed by addition of solid 2,6-di-O-methyl-β-cyclodextrin (Wako) in twofold molar excess[46]. For the acidification assay, we typically suspended 50 μl of liposomes (125 μg lipids, 2.5 μg $TF_0F_1$ and 5 μg VGLUT1) in 1 ml of assay buffer (100 mM potassium gluconate, 2 mM $MgSO_4$ and 5 mM MOPS, pH 7.3). Acridine orange, ATP and FCCP were added and data were recorded as described for synaptic vesicles. KCl (100 mM final) was included where indicated. VAL was added where indicated to a final concentration of 5 nM. The data were quantified as described for synaptic vesicles.

**Glutamate uptake.** 1–2 ml liposome suspension was applied to gel filtration onto Sephadex-25 columns (10–20-ml bed volume) to exchange the external anion as indicated. The standard uptake was measured at 32 °C with final concentrations of 4 mM ATP, 40 μM potassium glutamate, 10 mM potassium aspartate, 4 mM KCl and 2 μCi [$^3$H]-glutamic acid (GE) per data point (if not indicated differently in the figure legends) by addition of liposomes to a 10× reaction mixture. The reaction was stopped by flushing aliquots of 200–600 μl into 4 ml of ice-cold uptake buffer (100 mM potassium gluconate, 2 mM $MgSO_4$ and 5 mM MOPS, pH 7.3). The liposomes were then filtered through nitrocellulose membranes and washed three times with 4 ml of uptake buffer, and trapped radioactivity was counted by liquid scintillation. NIG, VAL and FCCP were included into the 10× reaction mixture where indicated to get final concentrations of 200 nM, 100 nM and 20 μM, respectively. Typically, 10–20 μg of reconstituted VGLUT1 were assayed per data point.

**Electron microscopy.** For negative staining, a solution containing liposomes was applied on a glow-discharged collodion-coated nickel grid, fixed with 4% paraformaldehyde and 0.5% glutaraldehyde in phosphate buffer (pH 7.4). The grids were washed with phosphate buffer and water and stained with 1.5% uranyl acetate (wt/vol). Grids were observed and imaged in a Hitachi H-7100 electron microscope at 75 kV.

**Data analysis and miscellaneous procedures.** All data in this study, including trace recordings, represent mean values of triplicate measurements, unless indicated differently in the figure legends. Confidence was assessed by either two-tailed unpaired or paired Student's *t* tests between datasets where indicated in the figure legends. Protein concentrations were measured with the BCA assay (Pierce). Purity of proteins was evaluated by SDS-PAGE and Coomassie blue staining. Mice were genotyped by PCR as described[25,26]. To compare protein levels in wild-type and mutant brain samples, equal amounts of protein were applied to SDS-PAGE gels and transferred on PVDF-membranes by standard procedures. Proteins were detected with corresponding primary antibodies and HRP-conjugated secondary antibodies (BioRad) using ECL (Perkin Elmer) and ChemidocXRS-J (BioRad). The resulting data were analyzed with Quantity One Software (BioRad). Mouse experiments followed protocols approved by the Institutional Animal Care and Use Committee of Tokyo Medical and Dental University.

*Note: Supplementary information is available on the Nature Neuroscience website.*

**ACKNOWLEDGMENTS**

We are grateful to M. Yoshida for donation of the DK8 strain carrying pTR19ASDS; S. Uchida and S. Sasaki for providing the *Clcn3*$^{-/-}$ mouse strain;

J.W. Szostak for pTAG2K; M. Hirosawa-Takamori and T. Takahashi for their technical assistance; and R. Jahn for encouragement during the course of this study and for critically reading the manuscript. This study was supported by a Grant-in-Aid for Scientific Research from the Japan Society for the Promotion of Science (17680032) and Takeda Science Foundation to S.T.

**AUTHOR CONTRIBUTIONS**

S.S. and S.T. designed the project. S.S. performed the experiments. S.S. and S.T. analyzed the data and wrote the manuscript. S.M.W. and N.B. generated the *Vglut1*$^{-/-}$ mice.

Published online at http://www.nature.com/natureneuroscience/
Reprints and permissions information is available online at http://www.nature.com/reprintsandpermissions/

1. Cidon, S., Ben-David, H. & Nelson, N. ATP-driven proton fluxes across membranes of secretory organelles. *J. Biol. Chem.* **258**, 11684–11688 (1983).
2. Xie, X.S. & Stone, D.K. Isolation and reconstitution of the clathrin-coated vesicle proton translocating complex. *J. Biol. Chem.* **261**, 2492–2495 (1986).
3. Moriyama, Y. & Nelson, N. The purified ATPase from chromaffin granule membranes is an anion-dependent proton pump. *J. Biol. Chem.* **262**, 9175–9180 (1987).
4. Schneider, D.L. The proton pump ATPase of lysosomes and related organelles of the vacuolar apparatus. *Biochim. Biophys. Acta* **895**, 1–10 (1987).
5. Xie, X.S., Stone, D.K. & Racker, E. Determinants of clathrin-coated vesicle acidification. *J. Biol. Chem.* **258**, 14834–14838 (1983).
6. Xie, X.S., Crider, B.P. & Stone, D.K. Isolation and reconstitution of the chloride transporter of clathrin-coated vesicles. *J. Biol. Chem.* **264**, 18870–18873 (1989).
7. Edwards, R.H. The neurotransmitter cycle and quantal size. *Neuron* **55**, 835–858 (2007).
8. Bellocchio, E.E., Reimer, R.J., Fremeau, R.T., Jr. & Edwards, R.H. Uptake of glutamate into synaptic vesicles by an inorganic phosphate transporter. *Science* **289**, 957–960 (2000).
9. Takamori, S., Rhee, J.S., Rosenmund, C. & Jahn, R. Identification of a vesicular glutamate transporter that defines a glutamatergic phenotype in neurons. *Nature* **407**, 189–194 (2000).
10. Maycox, P.R., Deckwerth, T., Hell, J.W. & Jahn, R. Glutamate uptake by brain synaptic vesicles. Energy dependence of transport and functional reconstitution in proteoliposomes. *J. Biol. Chem.* **263**, 15423–15428 (1988).
11. Naito, S. & Ueda, T. Characterization of glutamate uptake into synaptic vesicles. *J. Neurochem.* **44**, 99–109 (1985).
12. Bai, L., Xu, H., Collins, J.F. & Ghishan, F.K. Molecular and functional analysis of a novel neuronal vesicular glutamate transporter. *J. Biol. Chem.* **276**, 36764–36769 (2001).
13. Fremeau, R.T., Jr. *et al.* The expression of vesicular glutamate transporters defines two classes of excitatory synapse. *Neuron* **31**, 247–260 (2001).
14. Varoqui, H., Schäfer, M.K., Zhu, H., Weihe, E. & Erickson, J.D. Identification of the differentiation-associated $Na^+/P_i$ transporter as a novel vesicular glutamate transporter expressed in a distinct set of glutamatergic synapses. *J. Neurosci.* **22**, 142–155 (2002).
15. Fremeau, R.T., Jr. *et al.* The identification of vesicular glutamate transporter 3 suggests novel modes of signaling by glutamate. *Proc. Natl. Acad. Sci. USA* **99**, 14488–14493 (2002).
16. Hartinger, J. & Jahn, R. An anion binding site that regulates the glutamate transporter of synaptic vesicles. *J. Biol. Chem.* **268**, 23122–23127 (1993).
17. Tabb, J.S., Kish, P.E., Van Dyke, R. & Ueda, T. Glutamate transport into synaptic vesicles. Roles of membrane potential, pH gradient and intravesicular pH. *J. Biol. Chem.* **267**, 15412–15418 (1992).
18. Stobrawa, S.M. *et al.* Disruption of ClC-3, a chloride channel expressed on synaptic vesicles, leads to a loss of the hippocampus. *Neuron* **29**, 185–196 (2001).
19. Matsuda, J.J. *et al.* Overexpression of CLC-3 in HEK293T cells yields novel currents that are pH dependent. *Am. J. Physiol. Cell Physiol.* **294**, C251–C262 (2008).
20. Accardi, A. & Miller, C. Secondary active transport mediated by a prokaryotic homologue of ClC Cl- channels. *Nature* **427**, 803–807 (2004).
21. Picollo, A. & Pusch, M. Chloride/proton antiporter activity of mammalian CLC proteins ClC-4 and ClC-5. *Nature* **436**, 420–423 (2005).
22. Scheel, O., Zdebik, A.A., Lourdel, S. & Jentsch, T.J. Voltage-dependent electrogenic chloride/proton exchange by endosomal CLC proteins. *Nature* **436**, 424–427 (2005).
23. Graves, A.R., Curran, P.K., Smith, C.L. & Mindell, J.A. The $Cl^-/H^+$ antiporter ClC-7 is the primary chloride permeation pathway in lysosomes. *Nature* **453**, 788–792 (2008).
24. Friedrich, T., Breiderhoff, T. & Jentsch, T.J. Mutational analysis demonstrates that ClC-4 and ClC-5 directly mediate plasma membrane currents. *J. Biol. Chem.* **274**, 896–902 (1999).
25. Yoshikawa, M. *et al.* CLC-3 deficiency leads to phenotypes similar to human neuronal ceroid lipofuscinosis. *Genes Cells* **7**, 597–605 (2002).
26. Wojcik, S.M. *et al.* An essential role for vesicular glutamate transporter 1 (VGLUT1) in postnatal development and control of quantal size. *Proc. Natl. Acad. Sci. USA* **101**, 7158–7163 (2004).
27. Takamori, S., Riedel, D. & Jahn, R. Immunoisolation of GABA-specific synaptic vesicles defines a functionally distinct subset of synaptic vesicles. *J. Neurosci.* **20**, 4904–4911 (2000).
28. Takamori, S. *et al.* Molecular anatomy of a trafficking organelle. *Cell* **127**, 831–846 (2006).
29. Suzuki, T., Ueno, H., Mitome, N., Suzuki, J. & Yoshida, M. F(0) of ATP synthase is a rotary proton channel. Obligatory coupling of proton translocation with rotation of c-subunit ring. *J. Biol. Chem.* **277**, 13281–13285 (2002).
30. Wolosker, H., de Souza, D.O. & de Meis, L. Regulation of glutamate transport into synaptic vesicles by chloride and proton gradient. *J. Biol. Chem.* **271**, 11726–11731 (1996).
31. Roseth, S., Fykse, E.M. & Fonnum, F. Uptake of L-glutamate into rat brain synaptic vesicles: effect of inhibitors that bind specifically to the glutamate transporter. *J. Neurochem.* **65**, 96–103 (1995).
32. Winter, S. *et al.* Galphao2 regulates vesicular glutamate transporter activity by changing its chloride dependence. *J. Neurosci.* **25**, 4672–4680 (2005).
33. Juge, N., Yoshida, Y., Yatsushiro, S., Omote, H. & Moriyama, Y. Vesicular glutamate transporter contains two independent transport machineries. *J. Biol. Chem.* **281**, 39499–39506 (2006).
34. Burger, P.M. *et al.* Synaptic vesicles immunoisolated from rat cerebral cortex contain high levels of glutamate. *Neuron* **3**, 715–720 (1989).
35. Miesenbock, G., De Angelis, D.A. & Rothman, J.E. Visualizing secretion and synaptic transmission with pH-sensitive green fluorescent proteins. *Nature* **394**, 192–195 (1998).
36. Maycox, P.R., Hell, J.W. & Jahn, R. Amino acid neurotransmission: spotlight on synaptic vesicles. *Trends Neurosci.* **13**, 83–87 (1990).
37. Hansen, A.J. Effect of anoxia on ion distribution in the brain. *Physiol. Rev.* **65**, 101–148 (1985).
38. Price, G.D. & Trussell, L.O. Estimate of the chloride concentration in a central glutamatergic terminal: a gramicidin perforated-patch study on the calyx of Held. *J. Neurosci.* **26**, 11432–11436 (2006).
39. Takamori, S. VGLUTs: 'exciting' times for glutamatergic research? *Neurosci. Res.* **55**, 343–351 (2006).
40. Daniels, R.W. *et al.* Increased expression of the *Drosophila* vesicular glutamate transporter leads to excess glutamate release and a compensatory decrease in quantal content. *J. Neurosci.* **24**, 10466–10474 (2004).
41. Wilson, N.R. *et al.* Presynaptic regulation of quantal size by the vesicular glutamate transporter VGLUT1. *J. Neurosci.* **25**, 6221–6234 (2005).
42. Hell, J.W. & Jahn, R. in *Cell Biology: A Laboratory Handbook* 1st edn (ed. Celis, J.E.) 567–574 (Academic Press, New York, 1994).
43. Fujiyama, F., Furuta, T. & Kaneko, T. Immunocytochemical localization of candidates for vesicular glutamate transporters in the rat cerebral cortex. *J. Comp. Neurol.* **435**, 379–387 (2001).
44. Keefe, A.D., Wilson, D.S., Seelig, B. & Szostak, J.W. One-step purification of recombinant proteins using a nanomolar-affinity streptavidin-binding peptide, the SBP-Tag. *Protein Expr. Purif.* **23**, 440–446 (2001).
45. Chen, C. & Okayama, H. High-efficiency transformation of mammalian cells by plasmid DNA. *Mol. Cell. Biol.* **7**, 2745–2752 (1987).
46. Degrip, W.J., Vanoostrum, J. & Bovee-Geurts, P.H. Selective detergent-extraction from mixed detergent/lipid/protein micelles, using cyclodextrin inclusion compounds: a novel generic approach for the preparation of proteoliposomes. *Biochem. J.* **330**, 667–674 (1998).

Brief Communications

# Unique Luminal Localization of VGAT-C Terminus Allows for Selective Labeling of Active Cortical GABAergic Synapses

**Henrik Martens,[1] Matthew C. Weston,[2] Jean-Luc Boulland,[3] Mads Grønborg,[4] Jens Grosche,[5,6] Johannes Kacza,[7] Anke Hoffmann,[7] Michela Matteoli,[8] Shigeo Takamori,[9] Tibor Harkany,[10,11] Farrukh A. Chaudhry,[3] Christian Rosenmund,[2] Christian Erck,[1] Reinhard Jahn,[4] and Wolfgang Härtig[5]**

[1]Synaptic Systems GmbH, D-37079 Göttingen, Germany, [2]Department of Molecular and Human Genetics and Department of Neuroscience, Baylor College of Medicine, Houston, Texas 77030, [3]Biotechnology Centre of Oslo and Centre for Molecular Biology and Neuroscience, University of Oslo, N-0317 Oslo, Norway, [4]Department of Neurobiology, Max Planck Institute for Biophysical Chemistry, D-37077 Göttingen, Germany, [5]Paul Flechsig Institute for Brain Research, University of Leipzig, D-04109 Leipzig, Germany, [6]Interdisciplinary Center of Clinical Research (IZKF), Faculty of Medicine and [7]Department of Anatomy, Histology and Embryology, University of Leipzig, D-04103 Leipzig, Germany, [8]Department of Medical Pharmacology, National Research Council Institute of Neuroscience, University of Milan and Italian Research Hospital Don Gnocchi, I-20129 Milan, Italy, [9]Center for Brain Integration Research, Graduate School of Medicine, Tokyo Medical and Dental University, Bunkyo-ku, Tokyo 113–8519, Japan, [10]Department of Medical Biochemistry and Biophysics, Karolinska Institutet, S-17177 Stockholm, Sweden, and [11]Institute of Medical Sciences, College of Life Sciences and Medicine, University of Aberdeen, Aberdeen AB25 2ZD, United Kingdom

Neurotransmitter uptake into synaptic vesicles is mediated by vesicular neurotransmitter transporters. Although these transporters belong to different families, they all are thought to share a common overall topology with an even number of transmembrane domains. Using epitope-specific antibodies and mass spectrometry we show that the vesicular GABA transporter (VGAT) possesses an uneven number of transmembrane domains, with the N terminus facing the cytoplasm and the C terminus residing in the synaptic vesicle lumen. Antibodies recognizing the C terminus of VGAT (anti-VGAT-C) selectively label GABAergic nerve terminals of live cultured hippocampal and striatal neurons as confirmed by immunocytochemistry and patch-clamp electrophysiology. Injection of fluorochromated anti-VGAT-C into the hippocampus of mice results in specific labeling of GABAergic synapses *in vivo*. Overall, our data open the possibility of studying novel GABA release sites, characterizing inhibitory vesicle trafficking, and establishing their contribution to inhibitory neurotransmission at identified GABAergic synapses.

*Key words:* endocytosis; fluorescence detection; synaptic plasticity; vesicular GABA transporter; live cell imaging; synaptic vesicle

## Introduction

Quantal release of neurotransmitters, concentrated in synaptic vesicles (SVs) (Sudhof, 2004) undergoing activity-dependent exocytosis at synaptic active zones (Schoch and Gundelfinger, 2006), subserves neuronal communication at every synapse. Release of a neurotransmitter from SVs requires either a complete SV fusion and subsequent endocytosis recovering the vesicle membrane (Jahn, 1999), or a "kiss-and-run" mechanism with a transiently open SV fusion pore allowing neurotransmitter release into the synaptic cleft (Klingauf et al., 1998).

Vesicular neurotransmitter transporters (VNTs) shuttle neurotransmitters from the cytosol into SVs (Gasnier, 2000; Chaudhry et al., 2008a). VNTs, including those of glutamate (VGluT1–3) (Takamori, 2006), acetylcholine (VAChT) (Erickson et al., 1996a), monoamines (VMATs) (Erickson et al. 1996b; Liu and Edwards, 1997), and glycine/GABA (VGAT/VIAAT) (Chaudhry et al. 1998) exhibit characteristic substrate specificities and are often used as phenotypic neuronal markers (Takamori et al. 2000). Understanding the correct structure of VNTs is imperative to deduce their functional domains, to define their physicochemical properties, and to identify their domains transiently exposed on the plasmalemmal surface during SV fusion. Our knowledge on the transmembrane topology of VNTs is largely based on computer predictions, which propose cytosolic localization for both the N and C termini of all VNTs and an even number (6–12) of transmembrane domains (McIntire et al., 1997; Masson et al., 1999). Experimental data on VGAT partly support the model predictions by showing that GABAergic SVs can be selectively immunoisolated with antibodies raised against its cytosolic N-terminus extremity (Takamori et al., 2000).

To further resolve the transmembrane topology of VGAT we applied limited proteolysis, a method successfully used to map the topologies of other SV proteins (synaptophysin, synaptogyrin, synaptotagmin-1 [Syt1]). Accordingly, luminal epitopes,

Received Aug. 15, 2008; accepted Oct. 22, 2008.

This work was supported by the Bioprofile Program (BMBF; #0313132), EU Synapse (LSHM-CT-2005-019055), the Interdisciplinary Center of Clinical Research at the Faculty of Medicine of the Universität Leipzig (Z10), the Alzheimer's Association, and the Swedish Medical Research Council. We gratefully thank Matthias Böddener and Ute Bauer for technical help and Sonja Wojcik (Max Planck Institute for Experimental Medicine, Göttingen, Germany) for providing VGAT knock-out tissue samples.

This article is freely available online through the *J Neurosci* Open Choice option.

Correspondence should be addressed to Dr. Henrik Martens, Synaptic Systems GmbH, Rudolf Wissell Strasse 28, D-37079 Göttingen, Germany. E-mail: lab@sysy.com.

DOI:10.1523/JNEUROSCI.3887-08.2008

 0270-6474/08/2813125-07515.00/0

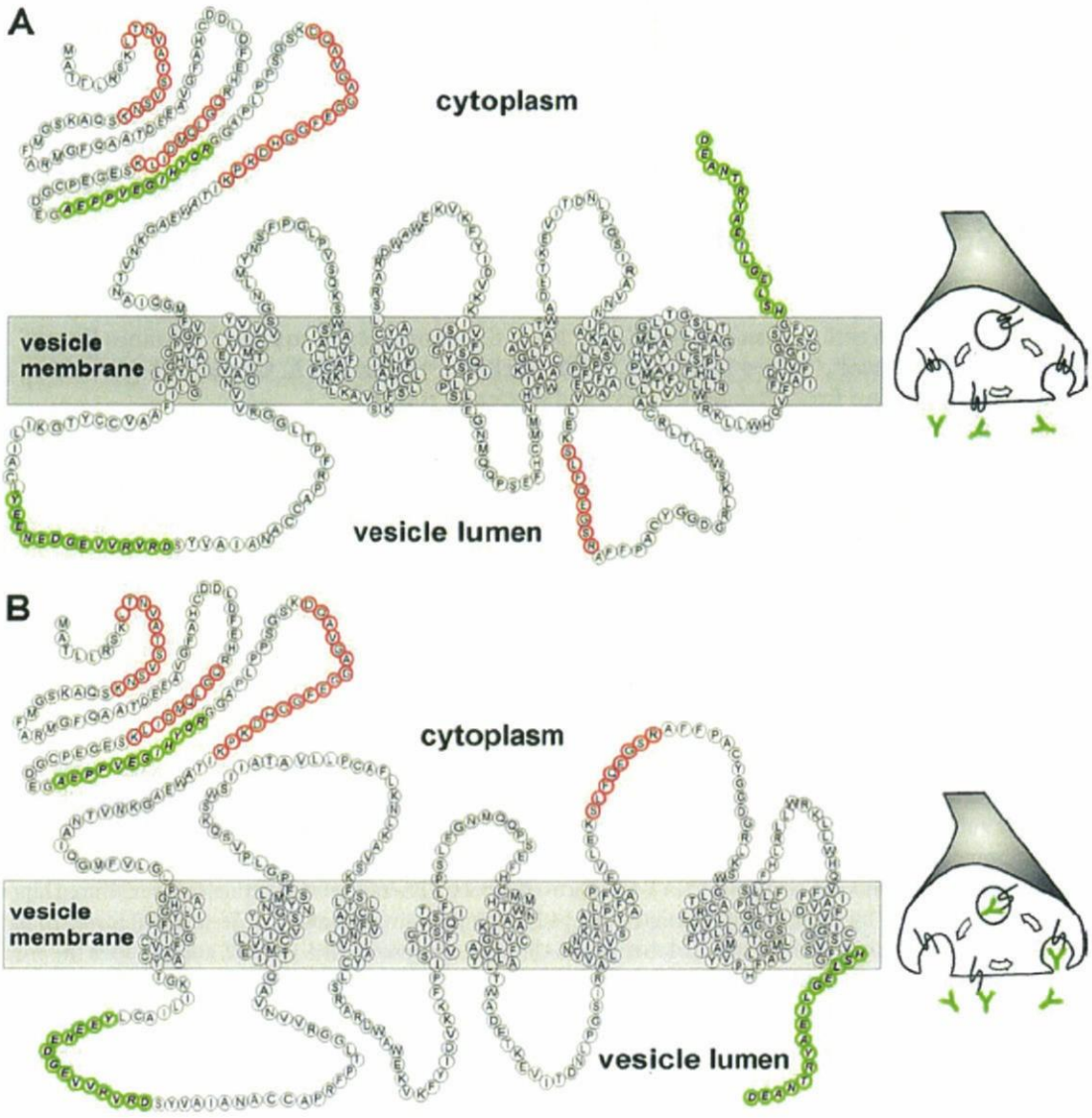


**Figure 1.** Refined transmembrane topology of VGAT. ***A***, Transmembrane structure of VGAT as proposed by McIntire et al. (1997) and as predicted by the TMHMM algorithm (***B***). Transmembrane domains are marked in gray. Epitopes in green were used to produce antibodies. Epitopes in red were detected by mass spectrometry. Insets denote the predicted exposure of luminal VGAT epitopes at the plasmalemmal surface and the likelihood of their targeting by antibodies during SV recycling.

e.g., the N terminus of Syt1 (Perin et al., 1991), are resistant to proteolytic cleavage as revealed by the molecular sizes of protected fragments by Western blotting (Stenius et al., 1995). In contrast, epitopes localized to the outer SV surface facing the cytosol, e.g., the N- and C-terminal endings of synaptogyrin and synaptophysin, are degradable. Here, we demonstrate that the C terminus of VGAT folds into the SV lumen. We also developed antibodies against short peptide sequences in (1) the N terminus, (2) the C terminus, or (3) the first luminal loop of VGAT (VGAT-N, VGAT-C, VGAT-lum1, respectively) (see Fig. 1) to elucidate the membrane topology of this protein, and to visualize forebrain GABAergic synapses both *in vitro* and *in vivo*. Similar to antibodies specific for the luminal domain of Syt1, which access the epitope during SV fusion and label endocytic vesicles (Kraszewski et al., 1995), fluorescent anti-VGAT-C targeting an intravesicular epitope allows the selective labeling of inhibitory presynaptic SV clusters during synaptic activity. Patch-clamp electrophysiology supports that anti-VGAT-C selectively recognizes VGAT. Collectively, our data elucidate a refined VGAT transmembrane topology and show that selective targeting of intraluminal VNT epitopes provides novel, effective means to label synapses of living neurons to establish their neurotransmitter phenotype *in vivo*.

## Materials and Methods

*Topology predictions.* Transmembrane domain predictions were performed using default settings of the TMHMM (Center for Biological Sequence Analysis, Technical University of Denmark, Lyngby, Denmark; http://www.cbs.dtu.dk/services/TMHMM) and HMMTOP algorithms (Hungarian Academy of Sciences, http://www.enzim.hu/hmmtop/), and the Tmpred service (http://www.ch.embnet.org/software/TMPRED_form.html). Models were compared with the structure reported by McIntire et al. (1997). Theoretical molecular weights of proteins and proteolytic fragments were calculated with the ProtParam tool (www.expasy.org; Swiss Institute of Bioinformatics, Basel, Switzerland).

*Antibodies and fluorochromation.* Commercially available antibodies are listed in supplemental material, available at www.jneurosci.org. Peptides corresponding to AA 510–525 (anti-VGAT-C) and AA 171–184 (anti-VGAT-lum1) of rat VGAT (McIntire et al., 1997) were synthesized

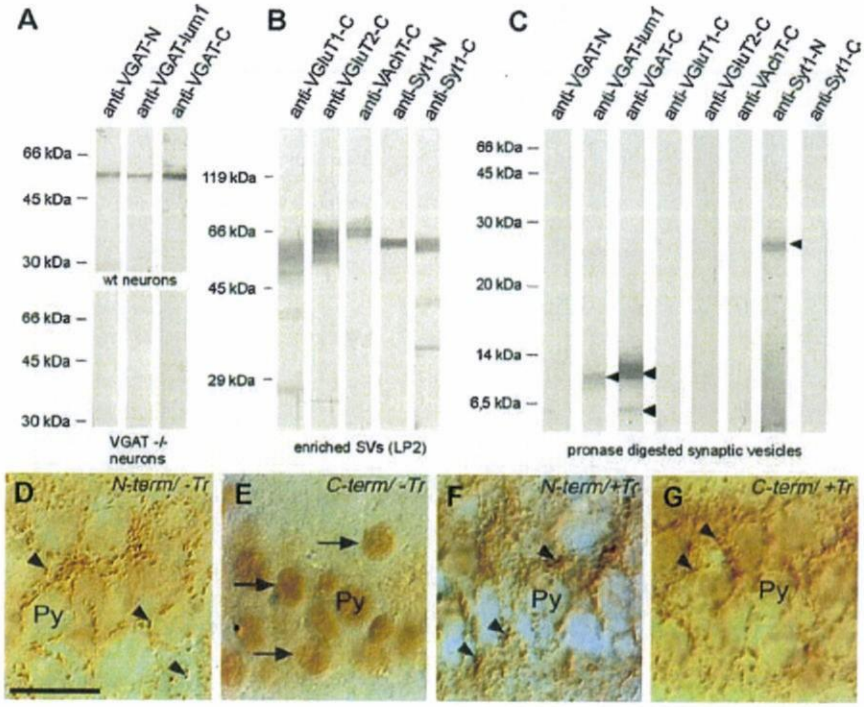


**Figure 2.** Epitope mapping of VGAT using domain-specific antibodies and limited SV proteolysis. ***A***, Comparison of antibodies raised against the N (VGAT-N) and C termini (VGAT-C), and the first luminal domain (VGAT-lum1) of VGAT by Western blotting of cell lysates from cultured wild-type (wt) and VGAT $^{-/-}$ hippocampal neurons. ***B***, Western analysis of enriched SVs (LP2) with antibodies recognizing the C termini of VGLUT1, VGLUT2, VAChT, the luminal N terminus (Syt1-N) and the cytoplasmic C terminus (Syt1-C) of Syt1. ***C***, Western analysis of proteolytic fragments (arrowhead) after pronase treatment of SVs. ***D–G***, Immunoperoxidase staining of VGAT-N and -C in hippocampal sections when luminal epitopes are concealed from or exposed to antibodies. Punctate terminal-like staining was detected around unstained pyramidal cells (Py) in the CA1 region by anti-VGAT-N both in the absence and presence of a detergent, respectively (arrowheads) (***D***, ***F***). Under identical staining conditions, anti-VGAT-C failed to reveal any terminal-like staining in the absence of a detergent even at high antibody concentrations causing aspecific nuclear staining (arrows) (***E***). Immunoperoxidase staining for VGAT-C with Triton X-100, which solubilizes membranes and facilitates antibody penetration into SV lumen, shows a punctate staining pattern resembling that obtained by anti-VGAT-N (***G***). Scale bar, 25 $\mu$m.

and coupled to keyhole limpet hemocyanin using standard procedures (Schneider et al., 1983). Antibodies were custom-generated (Biogenes) and affinity-purified using antigenic peptides immobilized on Sulfo-Link-Sepharose (Perbio) and are available from Synaptic Systems. Fluorochromation of affinity-purified anti-VGAT-C was performed following the manufacturers protocols (see supplemental material, available at www.jneurosci.org).

*Biochemistry.* Fractions enriched in synaptic vesicles (LP2) and pure SVs were prepared from adult Wistar rat brains according to Nagy et al. (1976). SDS-PAGE was used to detect full-length proteins (Laemmli, 1970). Pronase-digested SVs were separated by tricine SDS-PAGE to improve resolution in the low molecular range (Schägger and von Jagow, 1987). Each sample contained 200 $\mu$g of LP2 or 100 $\mu$g of pronase-treated SVs. Purified SVs (1 mg) were proteolytically digested with 200 $\mu$g of pronase (Sigma) in 2.5 ml of PBS (0.05 M, pH 7.4) for 3 h. Reactions were terminated by boiling the samples in SDS sample buffer containing 3% $\beta$-mercaptoethanol. Western blotting was performed according to Towbin et al. (1979). Mass spectrometry is described in supplemental material, available at www.jneurosci.org.

*Immunoperoxidase staining.* Immunoperoxidase staining of free-floating Vibratome sections was performed according to Chaudhry et al. (1998) (supplemental material, available at www.jneurosci.org).

*Cell culturing and VGAT uptake.* Primary hippocampal neurons were cultured according to Gauthier-Campbell et al. (2004). Internalization of fluorochromated antibodies was initiated by incubating neurons in Krebs-Ringer solution containing 55 mM KCl (Kraszewski et al., 1995) and polyclonal anti-VGAT-N, anti-VGAT-C or anti-VGAT-lum1 antibodies (5 $\mu$g/ml) at 37°C for 5 min. Cells were repeatedly washed in Krebs-Ringer buffer and subsequently in PBS. Images showing primary fluorochromated antibody binding were captured immediately. Unlabeled primary antibodies were detected after immersion fixation in 4% paraformaldehyde in PBS, blocking and permeabilization with PBS containing 3% BSA and 0.1% Triton X-100 for 20 min, and exposure to Cy3-tagged goat anti-rabbit IgG (1 h, 10–20 $\mu$g/ml, Jackson ImmunoResearch). Specific labeling was confirmed by co-staining with monoclonal anti-VGAT-N and Cy5-conjugated goat anti-mouse IgG. Details of CypHer5E-anti-VGAT-C uptake are in supplemental material, available at www.jneurosci.org.

*Electrophysiology.* Whole-cell patch-clamp recordings in hippocampal and striatal island cultures prepared from P0 mice were made according to Pyott and Rosenmund (2002) (supplemental material, available at www.jneurosci.org).

In vivo *labeling.* GABAergic terminals were labeled by stereotaxic injection of anti-VGAT-C into the hippocampi of anesthetized (33 $\mu$g/g; Hypnomidate, Janssen) young adult C57BL/6N mice. Surgery was performed as described (Siegemund et al., 2006) with 4 $\mu$g/2 $\mu$l anti-VGAT-C antibody injected at coordinates: AP = −2.2 mm, L = 1.9 mm, DV = 1.75 mm (relative to bregma). Mice were transcardially perfused 48 h later, and tissues processed according to Siegemund et al. (2006). *In vivo* labeling was analyzed in 30-$\mu$m-thick frozen sections as previously described for cholinergic neurons (Härtig et al., 1998). Labeling specificity was assessed by colocalization of Cy3- or Oyster550-anti-VGAT-C (2 $\mu$g/ml) and glutamate decarboxylase (GAD; 1:500), VGAT-N (1:50), parvalbumin (1:300) or synaptophysin (1:500; monoclonal IgGs). The absence of nonspecific *in vivo* labeling of glutamatergic fibers was shown by using guinea pig-anti-VGLUT1 (1:500; supplemental Table 1, available at www.jneurosci.org as supplemental material).

## Results

### Refined VGAT topology and verification by pronase mapping and mass spectrometry

McIntire et al. (1997) initially suggested a transmembrane VGAT structure with both termini facing the cytoplasm (Fig. 1*A*). Based on the TMHMM algorithm, we predicted an alternative transmembrane topology with the C terminus residing in the SV lumen being transiently exposed on the extracellular plasmalemmal surface during exocytotic fusion of SVs (Fig. 1*B*). We verified the transmembrane structure of VGAT by protease treatment of SVs followed by immunoblot analysis of the resulting fragments using epitope-mapped VGAT-N, VGAT-C and VGAT-lum1 antibodies (Fig. 1). Luminal, N- and cytoplasmic C-terminal tails of Syt1, and the C termini of VGLUT1, VGLUT2 and VAChT served as controls. Specificity of antibodies directed against three different epitopes of VGAT was confirmed by the findings that they recognized identical bands on cultured wild-type neurons but not on VGAT $^{-/-}$ material (Fig. 2*A*). Antibodies against VGLUT1, VGLUT2, VAChT and Syt1 revealed bands at the predicted molecular sizes (Perin et al., 1991, Stenius et al., 1995, Taka-